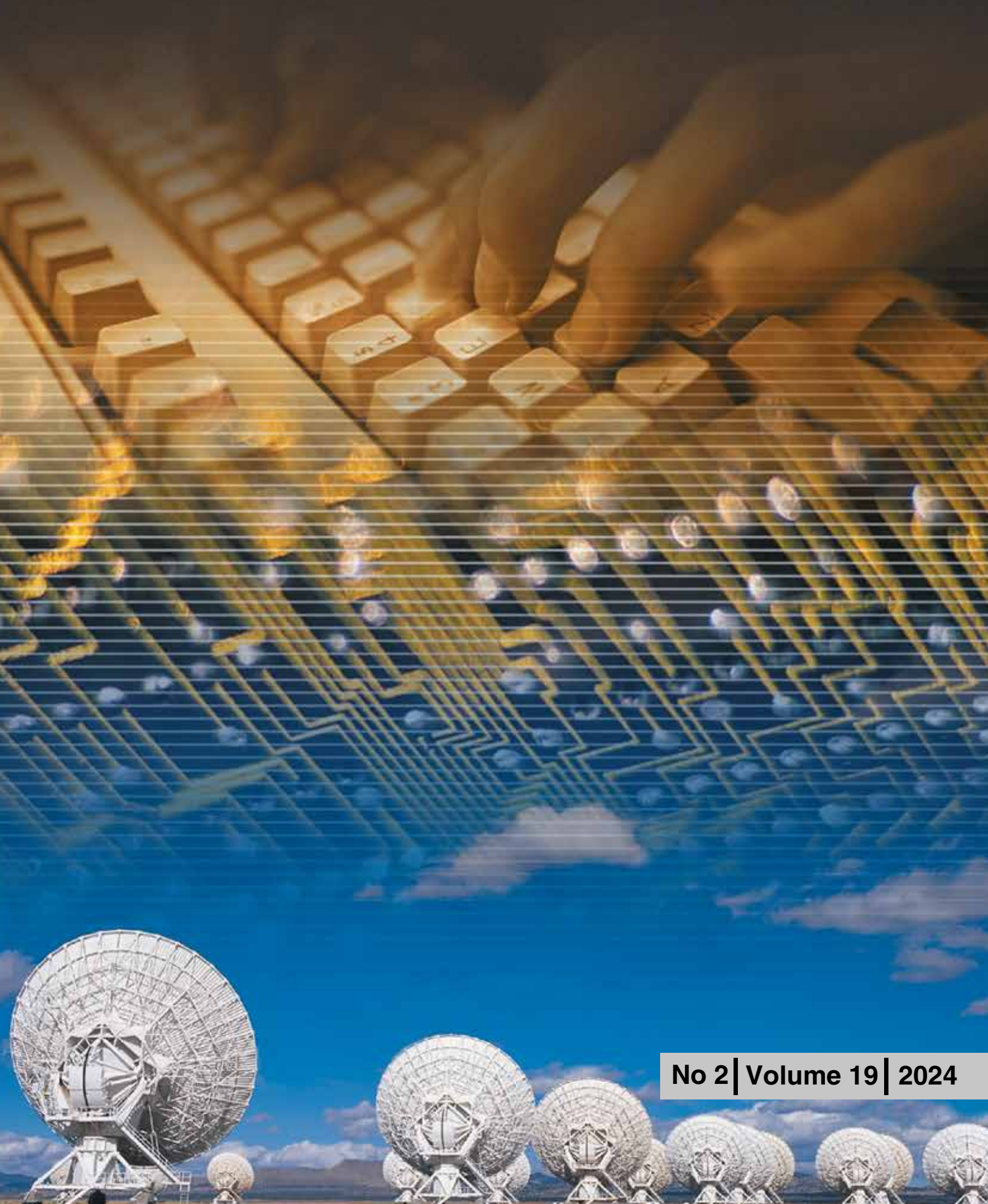


SCIENCE & MILITARY



No 2 | Volume 19 | 2024

The rationale for publishing this periodical by the Armed Forces Academy of General Milan Rastislav Štefánik is to enable the authors to publish their articles focused on particular scientific issues in the following areas: Military science, Natural Sciences, Engineering and Technology. Original scientific articles will be published twice a year.

Editorial Board

Chairman:

Brig. Gen. (ret.) Assoc. Prof. Eng. Boris **ĎURKECH**, CSc.

Armed Forces Academy of General M. R. Štefánik, Lipt. Mikuláš, SK

Members:

Prof. dr hab. Eng. Marek **AMANOWICZ**, PhD.

Military University of Technology, Warsaw, PL

Assoc. Prof. Eng. Vladimír **ANDRASSY**, PhD.

Armed Forces Academy of General M. R. Štefánik, Lipt. Mikuláš, SK

Col. Assoc. Prof. Eng. Milenko **ANDRIC**, PhD.

University of Defence in Belgrade, SRB

Assoc. Prof. Eng. Marián **BABJAK**, PhD.

Armed Forces Academy of General M. R. Štefánik, Lipt. Mikuláš, SK

Assoc. Prof. Eng. Július **BARÁTH**, PhD.

Armed Forces Academy of General M. R. Štefánik, Lipt. Mikuláš, SK

Brig. Gen. Prof. Eng. Ghita **BARSAN**, PhD.

„Nicolae Balcescu“ Land Forces Academy, Sibiu, RO

Prof. Eng. Dalibor **BIOLEK**, CSc.

University of Defence, Brno, CZ

Col. Prof. Vasile **CARUTASU**, PhD.

„Nicolae Balcescu“ Land Forces Academy, Sibiu, RO

Assoc. Prof. RNDr. Lubomír **DEDERA**, PhD.

Armed Forces Academy of General M. R. Štefánik, Lipt. Mikuláš, SK

Prof. RNDr. Anatolij **DVUREČENSKIJ**, DrSc.

Slovak Academy of Sciences, Bratislava, SK

Col. Assoc. Prof. Eng. Petr **FRANTIŠ**, Ph.D.

University of Defence, Brno, CZ

Prof. Eng. Karel **FRYDRÝŠEK**, Ph.D., Eng. - PAED IGIP

VSB Technical University of Ostrava, CZ

Prof. Eng. Jan **FURCH**, Ph.D.

University of Defence, Brno, CZ

Lt. Col. Assoc. Prof. Eng. Laurian **GHERMAN**, PhD.

„Henri Coanda“ Air Force Academy, Brasov, RO

Prof. Eng. Marcel **HARAKAI**, PhD.

Armed Forces Academy of General M. R. Štefánik, Lipt. Mikuláš, SK

Prof. C. S. **CHEN**

University of Southern Mississippi, US

Prof. Dr. Phill. Nat. Bernd **KLAUER**

Helmut Schmidt University, Hamburg, DE

Assoc. Prof. Eng. Peter **KORBA**, PhD. Eng. Paed. IGIP

Technical University of Košice, SK

Assoc. Prof. Eng. Mariana **KUFFOVÁ**, PhD.

Armed Forces Academy of General M. R. Štefánik, Lipt. Mikuláš, SK

Assoc. Prof. Eng. Michal **KVET**, PhD.

University of Žilina, SK

Assoc. Prof. Eng. Doru **LUCULESCU**, PhD.

„Henri Coanda“ Air Force Academy, Brasov, RO

Prof. Eng. Martin **MACKO**, CSc.

University of Defence, Brno, CZ

Prof. dr hab. Eng. Jędrzej **MACZAK**, PhD.

Military University of Technology, Warsaw, PL

Assoc. Prof. Eng. Branislav **MADOŠ**, PhD.

Technical University of Košice, SK

Maj. Gen. Assoc. Prof. Le Ky **NAM**

Military Technical Academy, Hanoi, VN

Dr. h. c. Prof. Eng. Pavel **NEČAS**, PhD., MBA

Matej Bel University in Banská Bystrica, SK

Assoc. Prof. Eng. Miloš **OČKAY**, PhD.

Armed Forces Academy of General M. R. Štefánik, Lipt. Mikuláš, SK

Col. Prof. Eng. Marian **PEARSICA**, PhD.

„Henri Coanda“ Air Force Academy, Brasov, RO

Assoc. Prof. Eng. Vladimír **POPADOVSKÝ**, PhD.

Armed Forces Academy of General M. R. Štefánik, Lipt. Mikuláš, SK

Brig. Gen. (ret.) Prof. Eng. Bohuslav **PŘIKRYL**, Ph.D.

Aerospace a. s., Praha, CZ

Assoc. Prof. Eng. Jozef **PUTTERA**, CSc.

Armed Forces Academy of General M. R. Štefánik, Lipt. Mikuláš, SK

Prof. Qinghua **QIN**

The Australian National University Canberra, AU

Prof. dr hab. Eng. Stanislaw **RADKOWSKI**, PhD.

Military University of Technology, Warsaw, PL

Assoc. Prof. Eng. Karol **SEMRÁD**, PhD.

Armed Forces Academy of General M. R. Štefánik, Lipt. Mikuláš, SK

Assoc. Prof. Eng. William **STEINGARTNER**, PhD.

Technical University of Košice, SK

Assoc. Prof. Eng. Mikuláš **ŠOSTRONEK**, PhD.

Armed Forces Academy of General M. R. Štefánik, Lipt. Mikuláš, SK

Assoc. Prof. Eng. Michal **TURČANÍK**, PhD.

Armed Forces Academy of General M. R. Štefánik, Lipt. Mikuláš, SK

Prof. Eng. František **UHEREK**, PhD.

Slovak University of Technology in Bratislava, SK

Assoc. Prof. Eng. Jiří **VESELÝ**, Ph.D.

University of Defence, Brno, CZ

Editor-in-Chief:

Brig. Gen. (ret.) Assoc. Prof. Eng. Boris **ĎURKECH**, CSc.

Armed Forces Academy of General M. R. Štefánik, Lipt. Mikuláš, SK

Executive editor:

Mgr. Anna **ROMANČÍKOVÁ**

Armed Forces Academy of General M. R. Štefánik, Lipt. Mikuláš, SK

Published by: Armed Forces Academy of General Milan Rastislav Štefánik, Demänová 393, 031 01 Liptovský Mikuláš, Slovak Republic. IČO 37 910 337. Registered No: EV 2061/08. ISSN 1336-8885 (print). ISSN 2453-7632 (online).

DOI: <https://doi.org/10.52651/sam.j.2024.2>

Printed by: EVOCOM, s. r. o., Strojárska 332/7B, 033 01 Podtureň, Slovak Republic.

Published biannually. The subscription rate for one year is 7,30 €.

The Journal Science & Military is included in following multiple databases: EBSCO. ProQuest Central: PQ Science Journals; PQ Military Collection; PQ Computing; PQ Telecommunications; Illustrata; Forthcoming Technology; Research Database (TRD) full text packages.

Address of the editorial office

Armed Forces Academy of General Milan Rastislav Štefánik, Demänová 393, 031 01 Liptovský Mikuláš,
Slovak Republic

Phone: +421-960-423065 E-mail: redakcia@aos.sk, <http://sm.aos.sk/index.php/en/>

© Armed Forces Academy of General Milan Rastislav Štefánik, Liptovský Mikuláš, December, 2024.

DOI: <https://doi.org/10.52651/sam.j.2024.2>

SCIENCE & MILITARY

No 2 | Volume 19 | 2024

*The Science & Military Journal is published in accordance with an Open Access (OA) under the **Creative Commons Attribution – NoDerivatives International License (CC BY-ND 4.0)** <http://creativecommons.org/licenses/by/4.0> .*



Dear Readers,

We are pleased to bring you the new issue of *Science & Military*. This peer-reviewed scientific journal strives for open access to scientific knowledge and its dissemination among the scientific community.

Today, open access is more than just a trend - it's a necessity. In the era, when information is available at our fingertips, it is our responsibility to ensure that knowledge is accessible to everyone, regardless of geographical or financial constraints. To this end, we strive to provide a platform where authors can share their research results with the global community. We aim to promote international cooperation and information exchange between countries, which is particularly important in the field of defence, where knowledge sharing can enhance global security. It can also increase transparency in the defence sector and strengthen public trust in military and government institutions. I would like to emphasise the fact that the contents and the insights published in *Science & Military* can be used outside the military environment as well.

Our ambition is not only to publish high-quality and innovative research papers, but also to be included in the prestigious Scopus database, which would be a big step forward for our authors and readers. Scopus is one of the largest databases of academic publications and provides access to a wide range of research articles, allowing researchers to follow trends and the work of other researchers in their field. Journals included in Scopus have greater visibility in the academic community, which can lead to increased citations and attention from researchers.

We firmly believe that our authors and readers will appreciate the benefits of open access. We hope our journal will go through a rigorous review process and be included in the SCOPUS database, which would certainly contribute to its further development and visibility.

Dear readers, let me briefly introduce the contents of the current issue:

The first among the peer-reviewed articles in this issue is the article titled **“A Design of 4-Lens Thermal Imaging Objective Working in the LWIR Spectral Region”** written by Chi Toan Dang and Van Bac Doan. The article documents the possibility of simultaneous active mechanical and passive optical compensation of the shift of the imaging plane of the thermal imaging objective when in a wide range of temperatures. The most important result described in the article is a way to design a lenticular thermal imaging objective that takes into account passive heat suppression, with which it is possible to work in the LWIR region.

Among the articles in this issue, you can find the paper written by Bence Hajós titled **“Some Additional Aspects for the Regulation of the Military**

Load Classification of Existing Road Bridges (STANAG 2021)”. This study examines some details of the regulation of load capacity assessment for military traffic on road bridges. The most significant results presented in the paper are the new crossing condition for continuous convoy movement, the proposed uniform marking system, and the revised safety factors.

The following article written by Vratislav Krehel, Michal Mozola and Martin Křepský titled **“Material and Technologies in the Design of Military Optical Devices”** deals with an analysis of the properties required to ensure the desired imaging quality, along with an overview of current and prospective modern materials suitable for constructing the bodies of optical devices.

Another paper titled **“Influence of Bullet Shape on .223 Remington Ammunition Accuracy Analysis”** was written by Tomáš Rázga, Peter Baláž, Michal Mozola and Vratislav Krehel. This article discusses the measured results of different bullet shape dispersions and possible causes of these adverse events. The most significant result presented in the paper is the evaluation of the bullet shape effect on the firing dispersion and accuracy.

The series of articles is closed with the paper titled **“Rocket Engine's Solid Propellants and Combustion Products”** written by Martin Křepský. This paper aims to analyse the chemical composition of various solid propellants for rocket engines and their performance. The most important is the analysis of combustion products for these propellants and their possible use for missile detection. The dependence of the spectral characteristics emitted or transmitted by combustion products can be used for the detection or possible identification of missiles.

Finally, on behalf of myself and the entire editorial board of *Science & Military*, I wish you a successful and productive New Year 2025. Let us not forget that science and research can profoundly shape our future. We are proud to be part of this journey that expands the boundaries of knowledge through open access.

Brig. Gen. (ret.) Assoc. Prof. Eng. Boris ĎURKECH, CSc.
Chairman of the Editorial Board

Reviewers

RNDr. Alojz **BAJČI**, CSc.
Armed Forces Academy of General Milan Rastislav Štefánik, Liptovský Mikuláš, SK

Prof. Dipl. Eng. Jiří **BALLA**, CSc.
Alexander Dubček University of Trenčín, Trenčín, SK

Dipl. Eng. Jan **KLESA**, Ph.D.
Czech Technical University in Prague

Assoc. Prof. Dipl. Eng. Michal **KRBAŤA**, PhD.
Alexander Dubček University of Trenčín, Trenčín, SK

Col Dipl. Eng. Jaroslav **KOMPAN**, PhD.
Armed Forces Academy of General Milan Rastislav Štefánik, Liptovský Mikuláš, SK

Prof. Dipl. Eng. Pavel **KONEČNÝ**, Ph.D.
University of Defence, Brno, CZ

Assoc. Prof. Dipl. Eng. Jaroslav **ODROBIŇÁK**, PhD.
University of Žilina, Žilina, SK

Assoc. Prof. Dipl. Eng. Ľuboš **OVSENÍK**, PhD.
Technical University of Košice, SK

LtCol Assoc. Prof. Dipl. Eng. Jiří **ŠTOLLER**, Ph.D.
University of Defence, Brno, CZ



A DESIGN OF 4-LENS THERMAL IMAGING OBJECTIVE WORKING IN THE LWIR SPECTRAL REGION

Chi Toan DANG, Van Bac DOAN

Abstract: This article presents a thermal imaging objective design with four lenses working in the LWIR (long-wave infrared) spectral region. The design solution combines passive heat removal and manual mechanical compensation. The optimization of the optical system quality is performed on ZEMAX optical software, taking into account the change in the operating temperature range of the optical system from -40 to +80 °C and the change in the image plane of the optical system compared to the detector. The change in the image plane of the optical system and the plane of the detector are then manually mechanically compensated. Considering criteria such as MTF (modulation transfer function), image spot size, energy function, the optical system has good image quality. Infrared materials are available on the market and the lens surfaces are completely spherical, so they are easy to manufacture and suitable for Vietnamese technology.

Keywords: Mechanical compensation; Optical compensation; Thermal infrared lens.

1 INTRODUCTION

Materials working in the 8-12 μm spectral region are characterized by high refractive index, low dispersion, and small amount. Aberrations common to infrared materials are corrected quite easily, except for the problem of thermal aberrations. Thermal aberration refers to the change in the image plane position of the optical system when the thermal imaging device works at different temperatures. The formula for determining the focal shift of a thin lens 1-element optical system according to temperature is calculated as follows [1, 3]:

$$\Delta f = \frac{f'}{(n-1)} \left(\frac{dn}{dt} \right) \Delta t, \quad (1)$$

where f' is the back focal length of the lens, n is the refractive index of the lens material, dn/dt is the change in refractive index with temperature, Δt is the working temperature difference of the lens. The focal shift increases proportionally to the change in refractive index. In addition, the wider the working temperature range, the larger the focal shift. There are many criteria to evaluate the quality of thermal imaging optical systems through evaluating the quality of the MTF (modulation transfer function), the RMS (root mean square) magnitude of the image spot, and the energy concentration function in an image pixel of the detector, Rayleigh standard of DOF (depth of focus),... In which, the magnitude of DOF is used to evaluate the quality of the optical system as expressed by the following expression [4, 6, 7]:

$$DOF = 4\lambda \cdot (f/\#)^2 = 4\lambda \cdot (f'/D)^2 \quad (2)$$

where $f/\#$ is the ratio of the back focal length to the clear aperture diameter, λ is the primary wavelength, D is the clear aperture diameter

of the objective lens. The depth of focus is proportional to the wavelength and proportional to the square of $f/\#$.

From formulas (1) and (2), it can be seen that, when the focus shift according to temperature exceeds the focus depth, the optical system does not satisfy the quality according to Rayleigh standards.

For example, for a lens of focal length $f' = 100$ [mm], made from Germanium material with $n = 4,001$ (at wavelength 10 [μm]), $dn/dt = 0.00039$, considering the temperature change range as from 0°C to +50°C, then $\Delta f' = 0.649$ [mm]. According to formula (2), considering the above lens when $f/\# = 3$, $DOF = 0.36$ mm. Thus, the above lens does not meet Rayleigh standards of quality. If one wants the optical system to achieve quality when the temperature changes, it is necessary to remove heat from the optical system, called athermalization. That is, adjusting the focus shift according to temperature so that the focus shift value is as small as possible.

There are two main methods for heat removal: mechanical and optical. The mechanical method is divided into two: active mechanical and passive mechanical. Passive mechanical methods rely on the natural expansion or contraction of mechanical parts to compensate for image displacement due to changes in working temperature.

The mechanical method actively adjusts by hand or uses motors and heat sensors to move the position of lenses as well as mechanical details and assemblies in the system. This method is widely used in zoom camera systems that require many different temperature compensation movements.

Passive optical methods rely on choosing a combination of optical materials to minimize the focus shift over a given temperature range [5]. The characteristic of this method is that there is little choice of materials, when good heat removal is required, it is necessary to use aspherical refractive surfaces or hybrid refractor/diffraction.

This article introduces the design of a heat-reducing thermal imaging objective optical system using the passive optical method, combined with a manual mechanical adjustment solution to ensure that the image plane of the optical lens coincides with the detector plane. This combination allows the design and manufacture of thermal imaging lenses in accordance with Vietnam's technological capabilities.

2 THEORETICAL CALCULATION BASIS AND SELECTION OF OBJECTIVE OPTICAL SYSTEM

2.1 Theoretical calculation basis

Select the objective lens focal length to be designed based on the parameters of the available detector, target size and required working distance. Then, the field of view of the objective lens is calculated according to the formula:

$$2\omega = \arctan\left(\frac{d}{f'}\right), \quad (3)$$

in which, f' is the back focal length of the objective lens, d is the diagonal of the detector matrix.

Select the parameter $f/\#$ according to the balance requirements of image illuminance, operating distance, and optical detail manufacturing technology. A value between 1.1 and 2.5 is reasonable. The optical clearance diameter of the objective lens is calculated according to the formula:

$$D = \frac{f'}{f/\#}. \quad (4)$$

Next, calculate the optical power of components based on the conditions of total optical power, chromatic aberration removal, and heat removal [2].

$$\phi = \sum_{i=1}^K \phi_i, \quad (5)$$

$$\sum_{i=1}^K \frac{\phi_i}{v_i} = 0, \quad (6)$$

$$\sum_{i=1}^K T_i \phi_i = -\alpha_h \phi, \quad (7)$$

in which, ϕ_i is optical power, v_i is the dispersion coefficient, T_i is thermal glass constant of the i -th component, respectively; ϕ is the total lens power, α_h is thermal expansion coefficient of the mounting base material; K is number of components.

2.2 Select the input criteria of the optical system

As mentioned in section 2.1, some basic parameters of the optical system are calculated and selected based on the working distance of the optical device, and also based on the features of the detector. It is assumed that the optical device can identify a human target at a distance up to 1500 meters, using a commercially available uncooled microbolometer detector. Table 1 shows the input parameters of the optical device.

Tab. 1 Table of optical input parameters of the objective lens

Parameter	Value
Detector dimensions, [$\mu\text{m} \times \mu\text{m}$]	640 x 512
Pixel size, [μm]	17
Working spectral range, [μm]	8 -12
f' , [mm]	100
2ω , [$^\circ$]	8
$f/\#$	1.2
Optical system length, [mm]	120

Source: authors.

3 RESULTS OF DESIGN AND ANALYSIS

From the formulas established above, combined with the selected detector, the optical power distribution of the components can be calculated, and the starting optical system can be selected.

After calculating the dimensions and finding the starting system, the optical system is imported into Zemax software for optimization. Enter the appropriate objective functions. First, optimize the optical system at a standard temperature of 25°C. Then, set up the optical system configuration working at nearby temperatures, and add the linear expansion coefficient of the mechanical material to make the objective tube (choose 2024 grade aluminum material with expansion coefficient $\alpha = 22.9 \cdot 10^{-6} [\text{mm}/(\text{mm} \cdot ^\circ\text{C})]$) [4]. The resulting objective lens optical system has the following configuration:

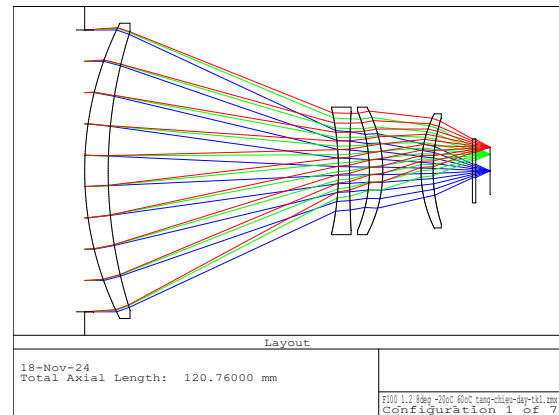


Fig. 1 Four-lens objective optical system

Source: authors.

The system consists of 4 lenses, of which the first and fourth lenses are made from germanium material, the second lens is made from ZnSe, and the third lens is made from ZnS. All above materials are popular and available on the market. To reserve a back focal length of the objective lens large enough for

assembly, a 1 [mm] flat plate made of Germanium was added.

The specific parameters of the designed optical system after multi-configuration optimization with working temperature of 25 °C and working pressure of 1 atmosphere are given in Table 2.

Tab. 2 Optimized objective parameters

Surf	Radius	Thickness	Glass	Semi-Diameter
STO	Infinity	0.00		42.00
2	97.58	7.00	GERMANIUM	44.00
3	135.63	68.60		41.48
4	-86.90	3.30	ZNSE	19.00
5	344.57	5.90		17.60
6	-46.93	4.00	ZNS IR	17.80
7	-40.69	11.40		19.00
8	38.95	3.60	GERMANIUM	17.00
9	52.68	11.70		15.78
10	Infinity	1.00	GERMANIUM	9.52
11	Infinity	4.26		9.41
IMA	Infinity			7.04

Source: authors.

In the extreme configurations with the operating temperature that differs the most from the standard operating temperature (the standard temperature is chosen to be 25 °C), the image quality of the optical system is the worst. Therefore, the following figures will describe the image quality of the optical system in three main configurations: the standard

configuration, two extreme configurations (operating temperature is -40 °C, and +80 °C).

The MTF curves of the optical system at different temperatures are shown in Figures 2-4.

The MTF value of the optical system at 25 °C is very good, the system quality is close to the diffraction limit.

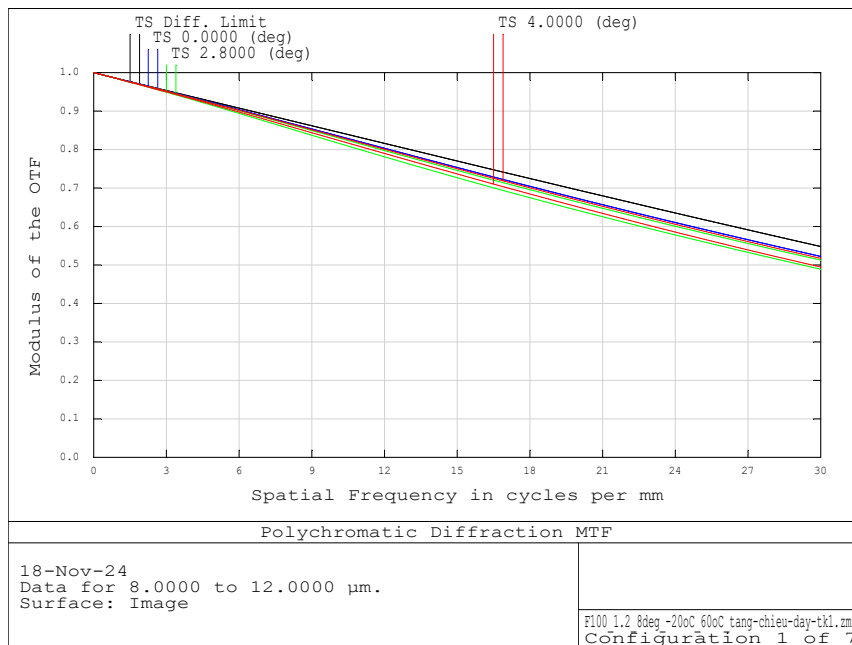


Fig. 2 MTF value of objective lens at 25 °C

Source: authors.

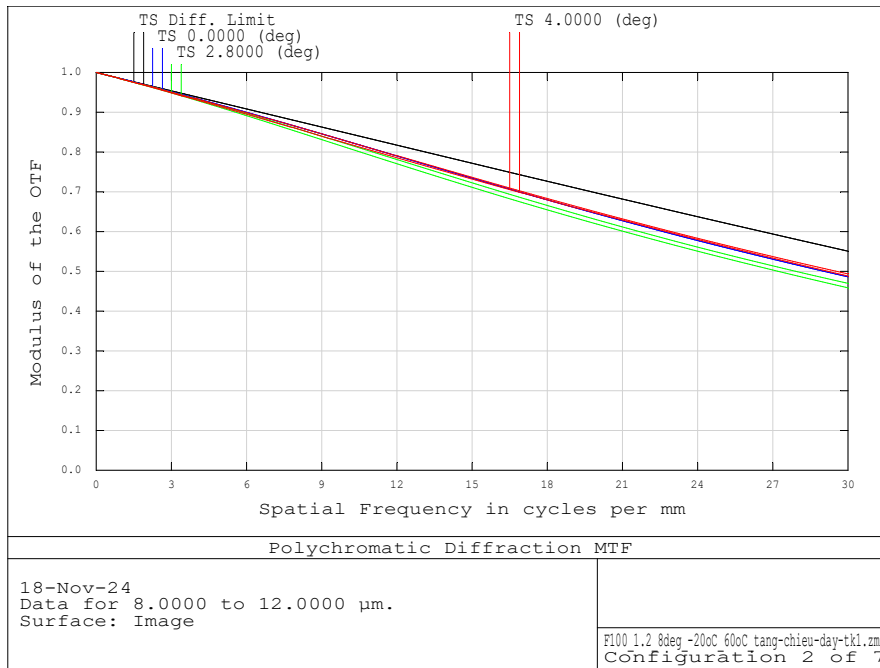


Fig. 3 MTF value of objective lens at -40 °C
Source: authors.

The MTF value of the optical system at -40 °C is lower than the MTF value at 25 °C, but is still quite

good. Similarly, the MTF value of the optical system at +80 °C also decreases.

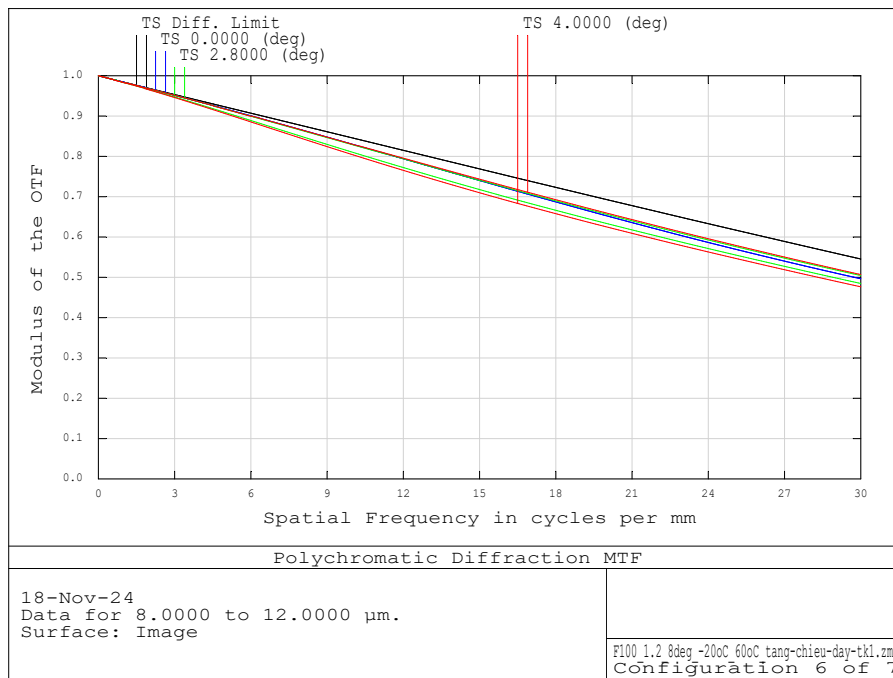


Fig. 4 MTF value of objective lens at 80 °C
Source: authors.

The image quality of the optical system is quite good, as shown by the MTF values being quite uniform throughout the entire working temperature range (-40 °C to +80 °C), all greater than 0.473 at the cutoff frequency of 30 [mm⁻¹]. The worst value is 0.458 at -40 °C (Figure 3).

The next pictures (Figures 5-7) show the shape and size of the image spot created by the objective optical system at different temperatures, the largest RMS image spot radius size is still smaller than the radius of the Airy disk, thus meeting the requirements for image spot quality.

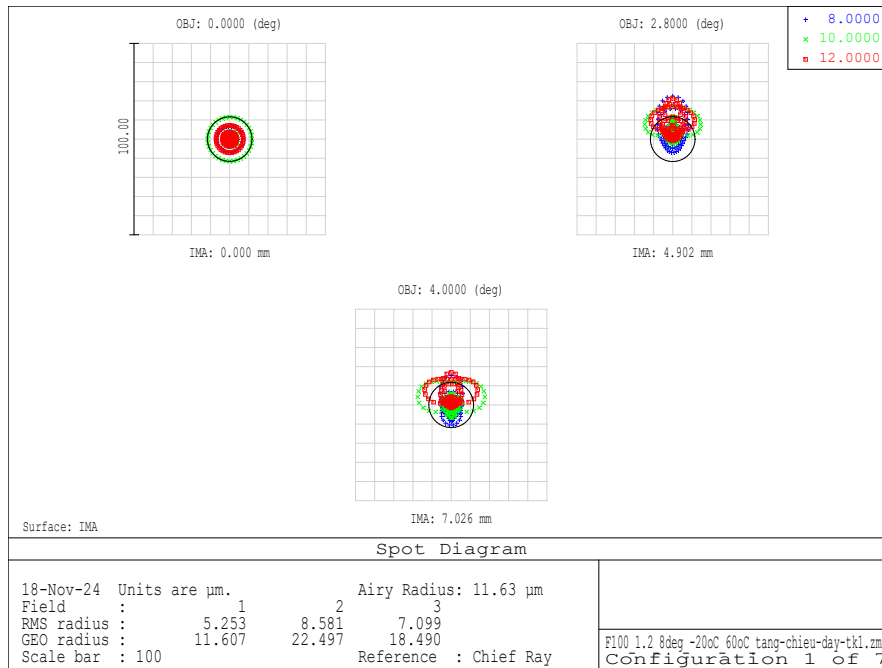


Fig. 5 RMS image spot size at 25 °C
Source: authors.

In Figure 5, the RMS radius of the image spot at the second field is the largest ($=8.581 \mu\text{m}$) and much smaller than the Airy disk radius, which proves that the image quality of the system at 25°C at the focal plane is very good.

In Figure 6, the RMS radius of the image spot at the third field is the largest ($=11.358 \mu\text{m}$) but is still smaller than the Airy disk radius ($=11.56 \mu\text{m}$).

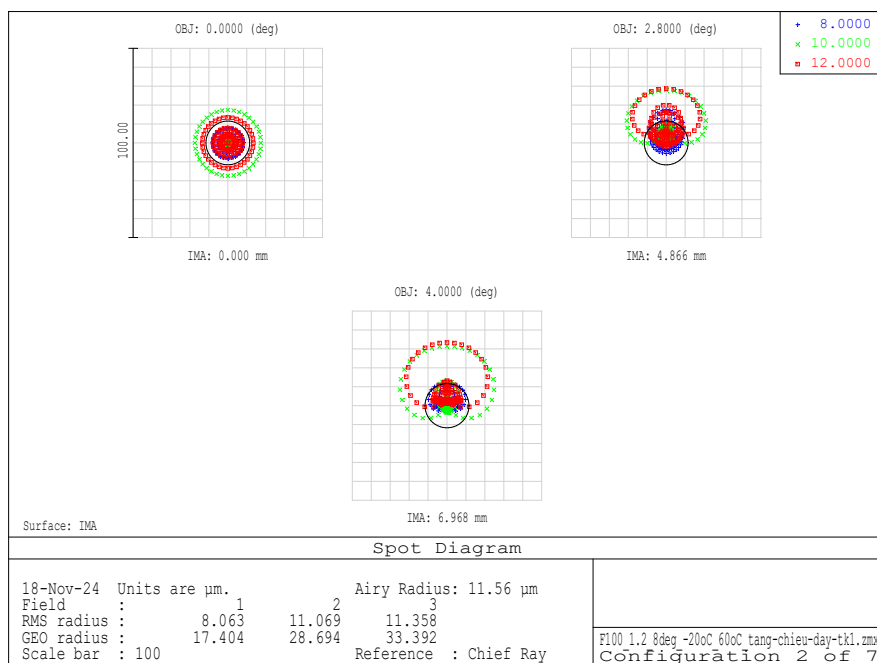


Fig. 6 RMS image spot size at -40 °C
Source: authors.

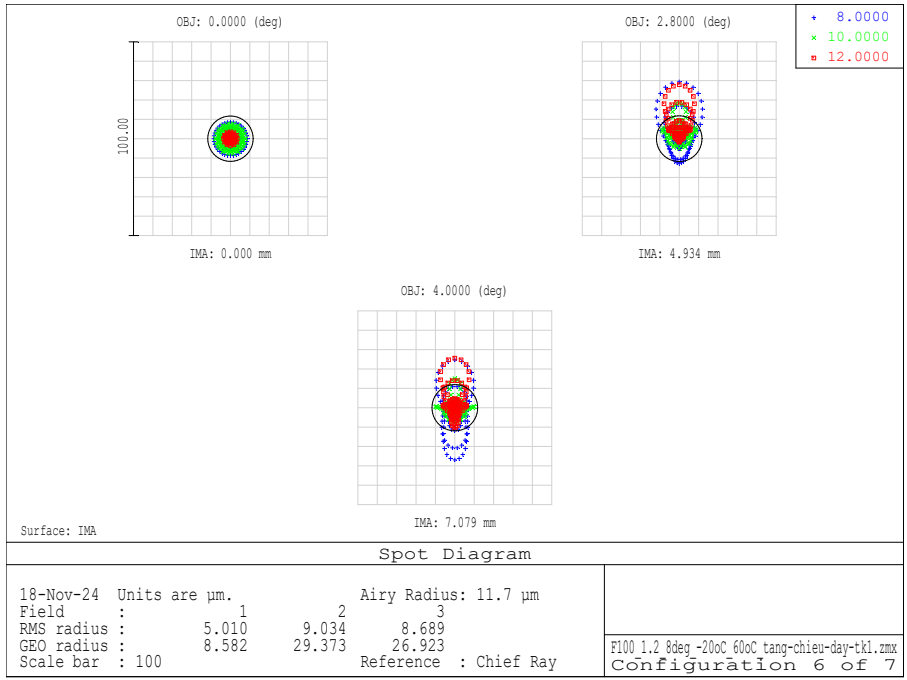


Fig. 7 RMS image spot size at 80 °C
Source: authors.

The graph representing the energy concentration function of the objective lens at different temperatures is shown in Figures 8-10, showing that the energy concentration function values are all

greater than 0.6 in a circle of radius 8.5 μm . Thus, about 60 % of the energy of the imaging beam lies entirely in one pixel of the detector.

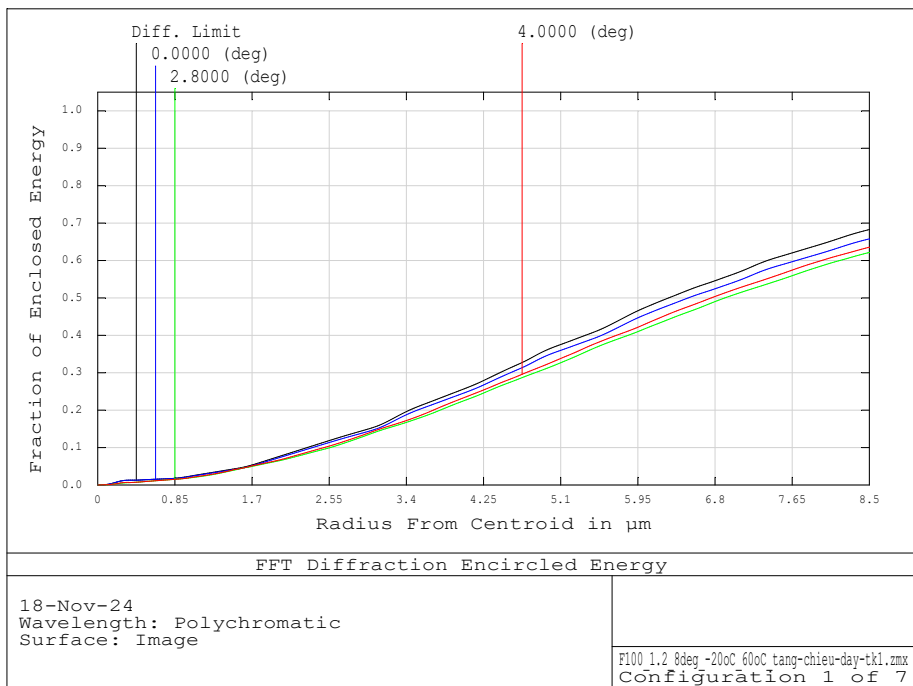


Fig. 8 Energy concentration function at 25 °C
Source: authors.

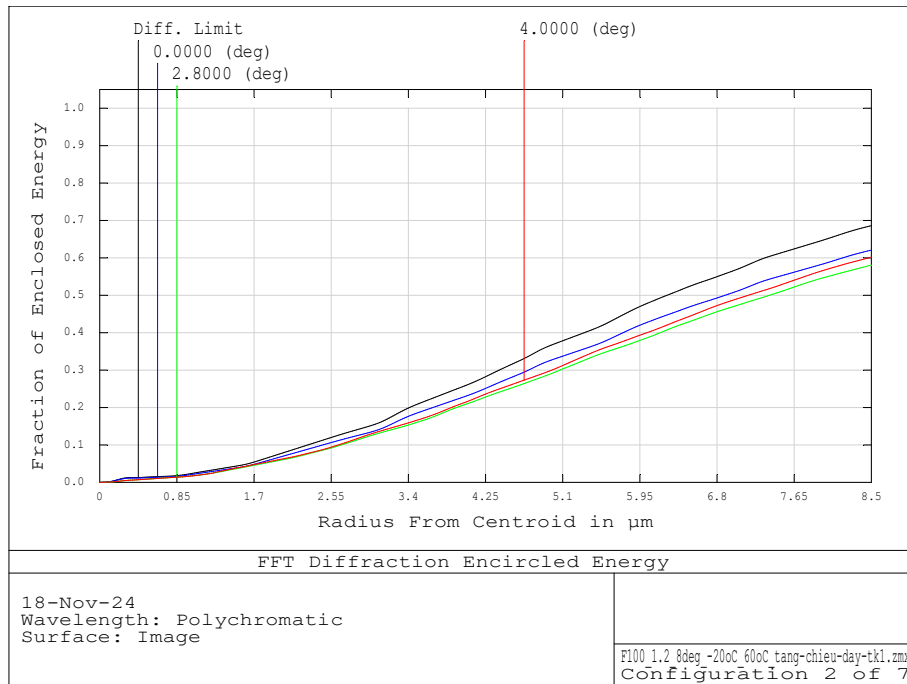


Fig. 9 Energy concentration function at -40 °C
Source: authors.

In Figure 9, the energy concentration function value at the second field (2.8 degrees) reaches 0.581 corresponding to 58.1 % of the light energy

concentrated in one pixel. This is the lowest energy concentration value of the optical system in the entire operating temperature range.

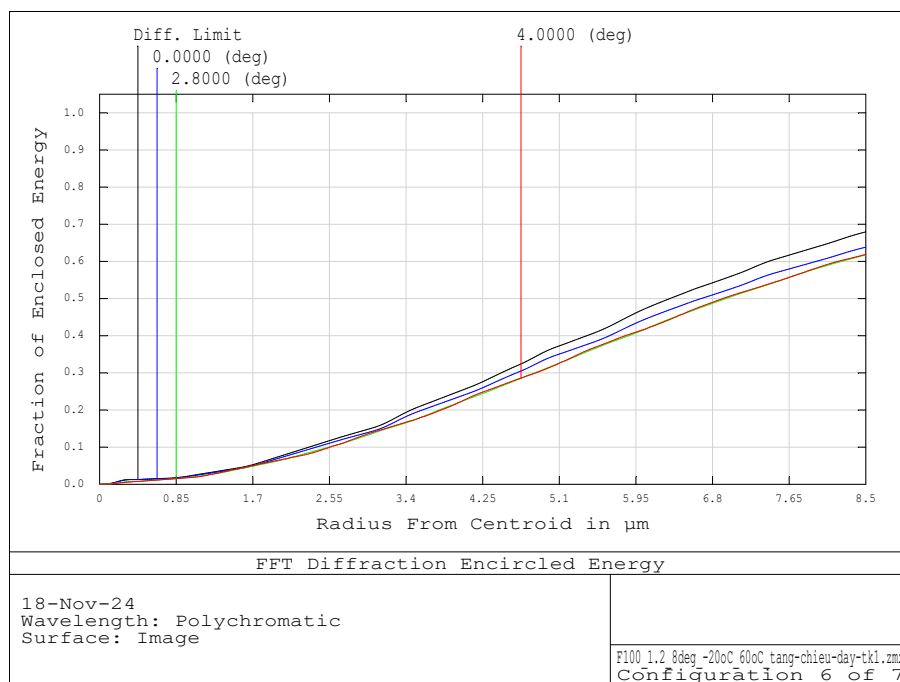


Fig. 10 Energy concentration function at 80 °C
Source: authors.

It is easy to see that at the extreme temperature of -40 °C, the optical system has the worst quality but is still acceptable (see Figures 3, 6, 9). Meanwhile, the optical system quality is best at the temperature of 25°C (see Figures 2, 5, 8). The optical system quality

at the remaining temperatures is better than at -40°C. Therefore, the system is capable of working in the temperature range from -40 °C to +80 °C.

The 3D drawing of the optimised objective lens optical system is shown in Figure 11.

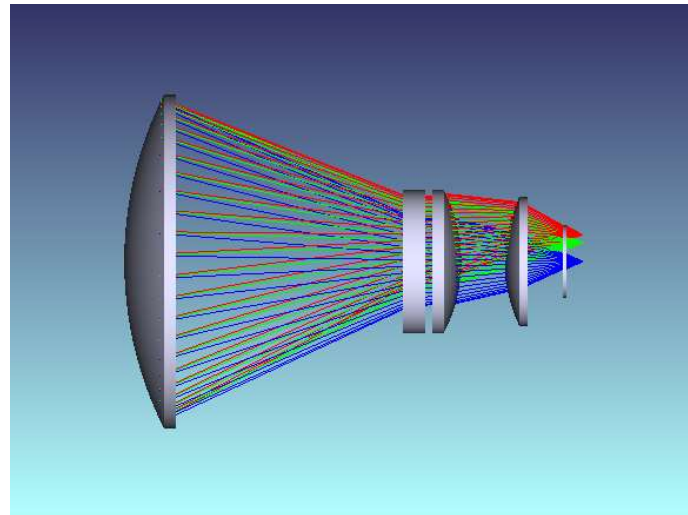


Fig. 11 3D drawing of the optimized objective lens optical system
Source: authors.

Consider one more criterion: the change in the image plane position of the objective lens. From the Lens Editor parameter table, extract the back focal

length of the objective lens in the entire working temperature range that has been optimized.

Tab. 3 Values of the back focal length of the objective lens according to the temperature

Configuration	1	2	3	4	5	6
Temperature	25 °C	-40 °C	-20 °C	0 °C	50 °C	80 °C
Back focal length	16.960	17.980	17.666	17.355	16.570	16.094

Source: authors.

Considering the temperature range from -20 °C to 80 °C, the largest back focal length value is 17,980 [mm] (at -40 °C) and the smallest is 16,094 [mm] (at 80°C). The difference in the back focal length value later is equal to 17,980-16,094=1,570 [mm]. The value is greater than the depth of focus, so to use this objective, it is necessary to re-calibrate the coincidence of the image plane with the detector plane. This is easily accomplished by an active mechanical solution when connecting the objective tube to the detector housing with a fine-pitch thread. The entire objective tube will be manually moved relative to the detector to coincide with the image plane of the objective lens and with the detector plane. This is a viable and cheap solution.

4 CONCLUSION

This article presents a method for designing a lens thermal imaging objective that takes into account the passive heat suppression that can work in the LWIR region. The optical system consists of four lenses that are completely spherical, convenient for processing. The materials used are commercially available. Active mechanical adjustment to coincide the image plane with the detector plane is completely feasible, so this type of objective lens can be designed and manufactured to serve the needs of observation,

detection, and identification. thermal target. To increase the quality of the optical system, it is necessary to continue to perform optimization with specialized optical software and it takes time.

References

- [1] ALLEN, M. *Infrared optics and zoom lenses*. Second edition. Bellingham, Washinton, USA: SPIE Press, 2009. Available at: <https://doi.org/10.1117/3.829008>
- [2] MAX J. RIEDL. *Optical design fundamentals for infrared systems*. Second edition. Bellingham, Washinton, USA: SPIE Press, 2001.
- [3] RICHARD C. JUERGENS. *Infrared optical systems*. OPTI 696, Practical optics seminar, 2006.
- [4] FISCHER, R. E., TADIC-GALEB, B. and YODER, P. R. *Optical system design*. Second edition. Mc Graw Hill: SPIE PRESS, 2008.
- [5] ROMANOVA, G. E. and PYS, G. *Research of aberration properties and passive athermalization of optical systems for infrared region*. Proc. Of SPIE Optical Systems Design,

Vol. 9626, 9626H-1, 2015. Available at:

<https://doi.org/10.1117/12.2191119>

- [6] SCHUSTER, N. and FRANKS, J. *Passive athermalization of two-lens-designs in 8-12 micron waveband*. Proc. Of SPIE Defense, Security and Sensing, Vol. 8353, 835325-1, 2012. Available at: <https://doi.org/10.1117/12.918112>
- [7] Zemax 13 Premium Programme. 2014.

Chi Toan **DANG**

University of Defence

Kounicova 65

662 10 Brno

Czech Republic

E-mail: chitoan.dang@unob.cz

Van Bac **DOAN**

Weapons Institute, GDDI

51 Phu Dien, Bac Tu Liem

Hanoi

Vietnam

E-mail: vanbacdoan@gmail.com

Chi Toan DANG was born in 1978. He graduated from Le Qui Don University of Technology, Hanoi, Vietnam in 2002 as an optical instrument engineer. He graduated with a Master's degree from Le Qui Don Technical University, Hanoi, Vietnam in 2018, majoring in optoelectronics. He worked in the optoelectronics factory, under the General Department of Defence Industry of Vietnam (2002-2011). Then he worked at the Weapons Institute of Vietnam, General Department of Defence Industry of Vietnam (since 2011). Currently, he is working as a doctoral student at the University of Defence, Brno, Czech Republic. Participated in optical processing technology, total installation of night vision devices, measurement, design of night vision lenses, and infrared lenses.

Van Bac DOAN was born in 1987. He got PhD degree from National Research University ITMO, Saint Petersburg, Department of Photonics and Optical Information Technology in 2018. He is now a researcher at the Weapons Institute, General Department of Defence Industry of Vietnam (GDDI). Participated in thin film coating technique, infrared materials research, design of day/night and thermal equipment.



SOME ADDITIONAL ASPECTS FOR THE REGULATION OF THE MILITARY LOAD CLASSIFICATION OF EXISTING ROAD BRIDGES (STANAG 2021)

Bence HAJÓS

Abstract: This study examines some of the details of the regulation of load capacity assessment for military traffic on road bridges. The author gives a proposal for modification of the standard. Suggestions include: definition of a new crossing condition, introduction of a uniform marking system, modification of the safety factor, improvement of the bending moment table of the standard and revision of the speed limit. These suggestions have certainly arisen in the application of local codes in some NATO countries. Maybe this open-source paper could be the first step to the professional discussion. In case of technical consensus, it is possible to incorporate the proposals (e.g. a new crossing condition) directly into STANAG.

Keywords: Military transport; Road bridges; Load capacity; Standards; STANAG 2021; AEP-3.12.1.5.

1 INTRODUCTION

The Achilles heel of military strategy is the logistics. Logistics is based on transport, which requires a good transport network. The most critical points in the network are typically bridges. The usability, adequacy and load-bearing capacity of bridges are therefore of paramount importance.

In Hungary, after joining NATO in 1999, the NATO standard AEP-3.12.1.5 [1] was introduced with STANAG 2021 [2], which provides for the load classification of bridges, ferries, rafts and military vehicles. The convention and the standard are in English, there is no official Hungarian translation.

The standard lays down a procedure for the classification of military vehicles according to their load and geometry, both wheeled and tracked. The second part of the standard provides for the classification of the load capacity of bridges, ferries and rafts. The purpose of the standard: if the classification number of a bridge or ferry or raft is greater than that of the military vehicle, there is no load obstruction to crossing [3].

The aim of the research is to develop the parameters and procedures necessary to extend the standard to Hungary. This is necessary because the standard gives national scope for the definition of partial factors, dynamic factors and other parameters that influence the assessment of load capacity (e.g. intensity of simultaneous civil traffic loads). This needs to be investigated on a national scale because their definition depends on the bridge design regulations of the country concerned. The aim of our work is to develop in detail a military load capacity conversion procedure derived from old Hungarian bridge design regulations [4].

On the basis of this studies we have carried out so far, we will provide some suggestions for supplementing and amending the existing standard. Among these, the main recommendations are the definition of a new crossing condition

and the elaboration of a standard notation of military classification. We then make three further suggestions for the standard.

According to the most commonly used design standards in NATO countries (e.g. EN, ASCI), a bridge is defined as any structure with a clear opening greater than 2 m. The study applies to all bridges (culverts, viaducts, overpasses, frames, ...).

2 ANALYSIS OF THE PROBLEM

The STANAG 2021 standard covers a very wide area. (Hereafter, we will refer to the Agreement and the underlying standard together as STANAG 2021. The text of the standard refers to itself as STANAG 2021.) It includes the classification of vehicles and the classification of bridges. A vehicle may cross a bridge if its classification number is less than the classification number of the bridge.

The Annex A of STANAG 2021 gives the ideal 16+16 vehicles for crawler (tracked) and tire cases (wheeled), which are the basis for military loads. The method of determining the load capacity may vary from country to country. In all cases, a dual load rating of road bridges should be carried out, giving the classification for tracked and wheeled vehicles separately. In the case of a simple one-span bridge structure, the tables and graphs for the classification of vehicles (Annexes B and C) may be used to calculate the classification of bridges.

We only deal with the classification of bridges. This is a big topic in itself, because it includes the methods that can be applied, from the simplest estimation (remote reconnaissance) to the most detailed investigation (even by test loading or destructive testing). We have limited our field of research to the A3c method according to the K.6.3 of the STANAG 2021.

The A3c method (correlation method) is sufficiently fast and reliable. The conversion procedure compares the bending moments and shear forces according to the bridge design standard with

the values according to STANAG 2021. To use this method, we need to know the construction, design load capacity of the bridge and use the old standard to which it was designed. The new aspects and proposals determined by the large number of calculations carried out are set out in Chapters 3-8.

3 PROPOSAL FOR A NEW CROSSING CONDITION

STANAG 2021 provides four different ways (cases) for civil and military vehicles to cross a road bridge (normal case with one lane of military traffic, normal case with two lanes of military traffic, caution case and risk case). Under normal loading, the ideal military vehicles are modelled as a convoy, with a distance of 30.5 m between successive vehicles. In the normal case, the military vehicles travel in one or two lanes and there is civilian traffic on the other lines of the bridge at the same time.

The standard defines the caution crossing and the risk crossing too. In the case of a caution crossing, there is a single vehicle on the bridge structure instead of a military convoy, with no simultaneous civilian traffic. The arrangement for a risk crossing is the same as for a caution crossing, but in this case minor damage to the bridge structure is allowed. The cases according to STANAG 2021 are shown in Figure 1.

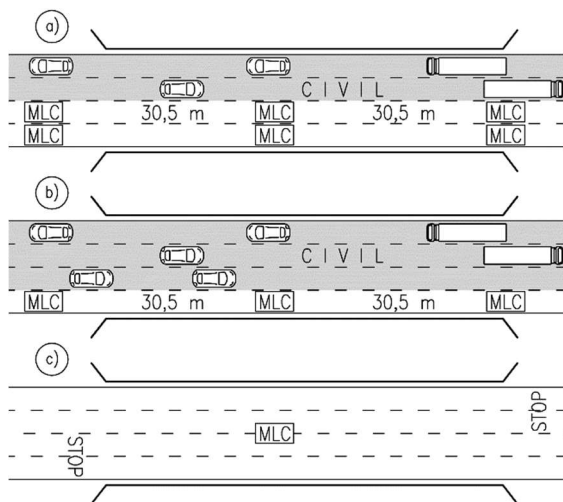


Fig. 1 Crossing conditions of the STANAG 2021
Source: author.

The difference between the normal cases and the other cases (caution and risk) is striking. This large difference naturally results in a large additional load capacity for caution and risk, but at the same time significantly limits military mobility due to the fact that the military convoy cannot move continuously.

Based on a detailed study of the standard and a number of test calculations, we propose to define and introduce a new crossing condition in the standard [5]. The new case is when the military

convoy is continuously moving on the bridge axis and there is no parallel civilian traffic (see Figure 2).

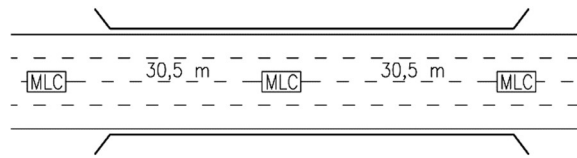


Fig. 2 Proposed new crossing conditions: Axis
Source: author.

It could be seen that this new case is very important for larger bridges, where several vehicles in a convoy can load the bridge at the same time. This is particularly important and useful for routes with many bridges.

We could take an example: if there are several long bridges on a route, the military vehicles can only cross them one at a time. This prevents the convoy from moving continuously and creates queues in the vehicle column that dramatically reduce the speed of the overall convoy.

For optimal military mobility, we propose to introduce the new case. We propose the term „Axis“ as the name of the new crossing condition. We were looking for a word that also has a different initial letter from the most important words used in the STANAG 2021 (Caution, Risk, Weheccle, Trucked, One, Two, Normal). This is important so that it cannot be confused with other important marker words and can easily be used as a short form or marking.

4 MARKING SYSTEM FOR BRIDGE LOAD CAPACITY

Under STANAG 2021, classified bridges are to be used by the entire NATO community. Therefore, it is of utmost importance that the load rating of the bridge is clear. Typically, a bridge will have more of load ratings. It should define the load capacity for wheeled vehicles and tracked vehicles separately. It should be defined for each crossing condition case. There are four types of crossing conditions in the standard, and we suggested a fifth in the previous chapter.

Two types of vehicles and five crossing conditions give us a total of 10 different load capacities for a single bridge. These 10 possible cases need to be clearly distinguished from each other. Unfortunately, we also encounter bad examples. The practice of specifying the load capacity of a bridge with a single number, for example MLC100, is wrong. We does not know which of the 10 possible cases the MLC100 value is used for.

Equally important is the methodology for the classification of the load capacity, which is regulated in detail in STANAG 2021. The classification methodology and the qualification of the person

performing the classification will influence the result and the usability of the classification.

We see that it is very important to accurately mark the load capacity of the bridge. For the marking system we have chosen the standard marking system for concrete as a model, [6]. We have developed a marking system for the load capacity of bridges [5], which we have improved with the new crossing

condition case proposed in the previous chapter (see Figure 3).

The precisely marked load capacity indicates, in addition to the nominal value of the load capacity, the vehicle type, the concurrency and the reliability of the determination (person and procedure). Without these parameters, the numerical value of the bridge load rating cannot be interpreted on its own.

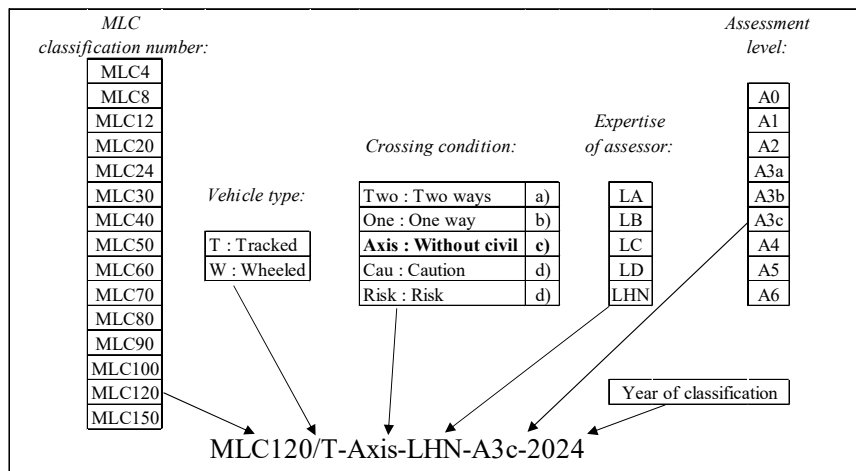


Fig. 3 Proposed making system of military load classification of bridges
Source: author.

The reliability part of the detailed marking gives you information on the usability. The general aim is that all bridges should have a specified load capacity of at least level A3c [5].

5 MODIFY OF SAFETY FACTORS

When classifying the load capacity of bridges, the safety factors, the dynamic factors, are national competences and can be defined by each country. The annex to the standard gives recommendations for these, giving values for the CC2 and CC3 importance classes, separately for the different military load groups (normal - caution - risk), and also distinguishing three short military design lifetimes (1 week, 4 weeks, 1 year) for the risk case - in clause K.8.6 [1]. This was published in the standard in 2017, see Tables 1 and 2 [1].

Tab. 1 Partial factors for assessment of CC3 bridges

CC3	Permanent Action	Variable Action
Normal	1.21	--
low dynamic	--	1.40
medium dynamic	--	1.50
Caution	1.21	1.26
Risk		
1 week	1.20	1.23
4 weeks	1.18	1.20
1 year	1.17	1.18

Source: [7].

Tab. 2 Partial factors for assessment of CC2 bridges

CC2	Permanent Action	Variable Action
Normal	1.19	--
low dynamic	--	1.33
medium dynamic	--	1.40
Caution	1.19	1.22
Risk		
1 week	1.18	1.19
4 weeks	1.16	1.16
1 year	1.16	1.16

Source: [7].

These factors were published in 2014 [7]. The theoretical derivation of the factors is discussed in detail in the thesis just quoted. One basis for the derivation is a graph from Eurocode [8]: Reliability levels for different reference periods in accordance (see Figure 4).

Figure 4 shows that a shorter design life is associated with a higher reliability level. This should be interpreted as being true for the same structure (resistance) and/or for the same load (impact). For example, a probability of failure of 50 years is calculated by summing the probability over one year as 50 consecutive independent events, of which if one occurs the bridge will fail. Thus, for longer durations, the probability of failure increases, and Beta (reliability level) decreases.

When judging the military load capacity, the reliability level should not be derived from

the design life, but from the needs determined on the basis of probabilistic considerations. If these external conditions are the same and only the design life is different (because the operational plan requires a bridge to be in place for only one week or one year), then the reliability level will be the same.

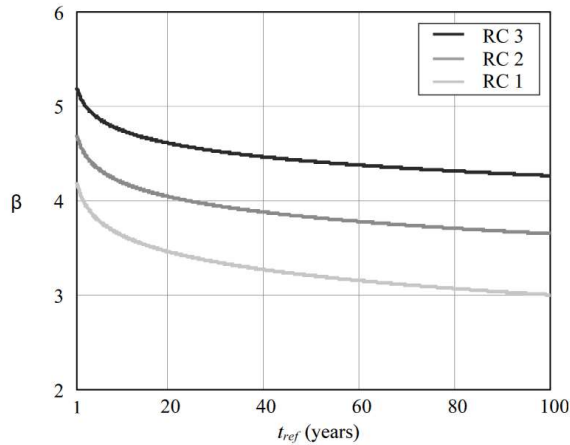


Fig. 4 Reliability levels for different reference periods Source: [8].

The same can be found in the dissertation [7]. It states that Beta does not change the lifetime of the structure (see Table 3).

Tab. 3 Target reliabilities for Risk Crossing Condition

Consequence class	Time reference	β_{hs} human safety	β_0 structural safety	max
CC3	1 week	3.4	2.8	3.4
	4 weeks	3.0	2.8	3.0
	1 year	2.0	2.8	2.8
CC2	1 week	2.9	2.4	2.9
	4 weeks	2.4	2.4	2.4
	1 year	1.3	2.4	2.4

Source: [7].

We could look at a simple example: We need a Beta=3 reliability level for Bridge ‚A‘ for only one week, and we also need a Beta=3 reliability index for Bridge ‚B‘ for a design life of one year. Obviously, the equal Beta and the safety factor derived from the cost optimisation result will be lower for Bridge ‚A‘ than for Bridge ‚B‘, because the probability of the effect occurring will be lower over the shorter time. And as a result, we can demonstrate an effectively larger military payload on Bridge ‚A‘ than on Bridge ‚B‘.

This statement contains a lot of simplifications. The probability of a significant effect is not only a function of time. It is possible for a bridge to be used for only one week, but to have continuous and intense traffic. It is also possible for a bridge to be used for a year, but the expected traffic is close to zero. The statistically influencing parameters are uncertain

and therefore we can simplify by using only the design time.

The example shown is contrary to the factors in the standard in the Risk case! Other contradictions are possible from the parameters in the standard: a bridge does not meet a design life of 1 week, but meets a design life of 1 year.

Our suggestion is to adopt the factors for the 1 year design life in the standard with the same value for shorter design lives. This way, the lack of correction of the factors remains in favour of safety. If one calculates with the wrong or old factors, one only errs in the direction of safety. The factors for 1 year can be accepted as factors independent of design life (see Table 4).

The factors for the payload were determined by taking 1.5 as the initial, original value (which appears in the table for CC3 as the maximum value). The safety factor for a payload vehicle in Hungary is 1.35 according to the Eurocode in force. We have therefore added the value of the original factor to the table. If the original factor was 1.35, then the values in the variable action* column should be used. In this column, we have entered the factors using a simple proportionalisation due to the difference between 1.5 and 1.35.

Tab. 4 Proposed safety factors for assessment of CC2 bridges

CC2	Permanent Action	Variable Action	Variable Action*
Original	1.35	1.50	1.35
Normal low dyn. medium dynamic	1.19	--	--
	--	1.33	1.23
	--	1.40	1.28
Caution	1.19	1.22	1.15
Risk	1.18	1.19	--
	1.16	1.16	--
	1.16	1.16	1.11

Source: author.

6 SMALL CORRECTION IN THE BENDING MOMENTS OF TRACKED VEHICLE

Annex B of STANAG 2021 gives the bending moments and shear forces in tabular form as a function of span. Annex C contains the same in graphical form. For wheeled vehicle data, the constant values for the small support spacing are shown, which is derived from the load on a single axle specified for loads. The same is not found at the tracked vehicles.

For tracked loads, STANAG 2021 Chapter 6.4.4.2 requires that the single axle load half value for the vehicle category shall be taken into account as the

local load. The effect of this is significant for small support distances, similar to wheeled vehicles.

The table of bending moments for MLC30 - MLC150, improved by the solo axle effect as required by the standard, is shown in Table 5. It can be seen that the largest difference is for the MLC150, where the solo axle is the standard up to 2 m span. The graph corrected according to the table is shown in Figure 5, which can be used as a correction to the STANAG 2021 Annex C Figures C-6 and C-7.

In terms of shear force, the required solo axle does not cause any major stress in any load class.

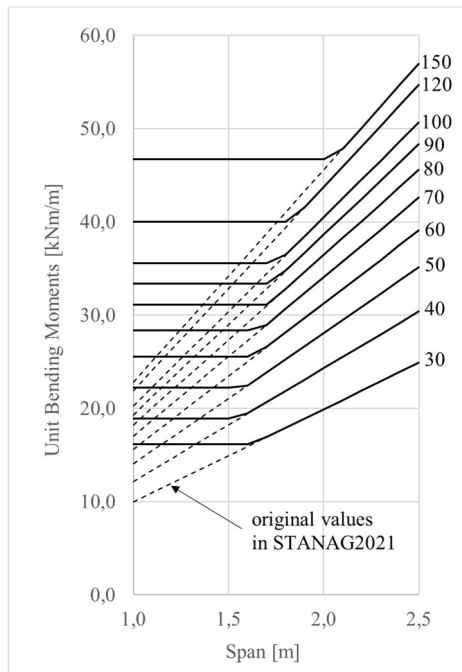


Fig. 5 Modified graph of bending moments
Source: author.

7 REVIEW OF THE SPEED OF MILITARY VEHICLES

STANAG 2021 regulates the speed of military vehicles in two places, in Annexes H and Annex K. Unfortunately, the values given in Caution case are contradictory (see Table 6).

Speed is an important parameter in military transport. Another problem about the Table 6, apart from the contradiction, is that it general imposes a speed limit on bridges. Modern vehicles are capable of faster speeds. The requirement under STANAG 2021 thus results in a mandatory speed limit on all bridges.

The speed of the vehicle affects the dynamic effect. Many studies have looked at the dynamic effects of military vehicles, [9] [10]. Dynamic coefficient can be reduced for tracked vehicles and heavy equipment trailers. It has been shown that the dynamic effect decreases proportionally with increasing vehicle mass [11].

Overall, the speed limit will improve the load capacity of bridge slightly, but will slow down military traffic considerably. Speed restrictions for military traffic are not desirable.

We would recommend deleting the speed limit of normal crossing condition in Annex K of STANAG 2021. The Caution case requires detailed consideration. Further investigation is needed to determine whether the removal of the speed limit in the Caution case would significantly reduce the available load capacity. It would be desirable to remove the speed limit in the Caution case (similar to the Axis crossing condition proposed in Chapter 3).

In the case of Risk, there is no contradiction in STANAG 2021 and it is recommended to maintain the 5 km/h speed limit.

Tab. 5 Modified table of the bending moments for tracked vehicle

L [m]	MLC30	MLC40	MLC50	MLC60	MLC70	MLC80	MLC90	MLC100	MLC120	MLC150
1	16,12	18,90	22,24	25,57	28,35	31,14	33,35	35,59	40,04	46,70
1,1	16,12	18,90	22,24	25,57	28,35	31,14	33,35	35,59	40,04	46,70
1,2	16,12	18,90	22,24	25,57	28,35	31,14	33,35	35,59	40,04	46,70
1,3	16,12	18,90	22,24	25,57	28,35	31,14	33,35	35,59	40,04	46,70
1,4	16,12	18,90	22,24	25,57	28,35	31,14	33,35	35,59	40,04	46,70
1,5	16,12	18,90	22,24	25,57	28,35	31,14	33,35	35,59	40,04	46,70
1,6	16,12	19,45	22,47	25,57	28,35	31,14	33,35	35,59	40,04	46,70
1,7	16,93	20,66	23,87	26,56	28,96	31,14	33,35	35,59	40,04	46,70
1,8	17,93	21,88	25,27	28,13	30,66	32,81	34,78	36,46	40,04	46,70
1,9	18,92	23,09	26,68	29,69	32,36	34,64	36,71	38,49	41,57	46,70
2	19,92	24,31	28,08	31,25	34,07	36,46	38,64	40,51	43,75	46,70
2,1	20,91	25,52	29,49	32,81	35,77	38,28	40,57	42,54	45,94	47,85
2,2	21,91	26,74	30,89	34,38	37,47	40,11	42,51	44,56	48,13	50,13
2,3	22,91	27,95	32,29	35,94	39,18	41,93	44,44	46,59	50,32	52,41
2,4	23,90	29,17	33,70	37,50	40,88	43,75	46,37	48,61	52,50	54,69
2,5	24,90	30,38	35,10	39,07	42,58	45,58	48,30	50,64	54,69	56,97

Source: author.

Tab. 6 Speed limit in the STANAG 2021

Annex	Crossing Condition		
	Normal	Caution	Risk
H.1. and H.2. (in text)	--	5 km/h	5 km/h
K.8.3. (part of Table 5.)	MLC ≤ 30 : 40 km/h MLC > 30 : 25 km/h	MLC ≤ 30 : 25 km/h MLC > 30 : 15 km/h	5 km/h

Source: [1].

8 SUMMARY

The use of a common standard, STANAG 2021, is necessary for the uniformity of the military load rating of road bridges. The classification of the load capacity of bridges is influenced by the inclusion of certain parameters.

We have formulated five suggestions for modifications to the use of the standard, which we propose for further analysis and consideration.

In case of a professional consensus, we propose to improve the standard by adding the amendments discussed here. The most important of our proposals, and the one that would be of most practical help in using STANAG 2021, would be the introduction of a uniform detailed marking system, for which we have developed a detailed proposal.

References

- [1] AEP-3.12.1.5 NATO Standard Military Load Classification of bridges, ferries, rafts and vehicles. Edition A Version 1, September 2017.
- [2] STANAG 2021 Standardization Agreement, Military Load Classification of bridges, ferries, rafts and vehicles. Edition 8, 14 September 2017 NSO/1074 (2017) MILENG/2021.
- [3] GULYÁS, A. Az érvényben lévő hídtervezési előírások és a hidak terhelési osztályba sorolása a STANAG 2021 szerint. In *Műszaki Katonai Közlöny*, 2002, 12(1–2), pp. 53–68.
- [4] GULYÁS, A. and HAVASI, Z. Hidak terhelési osztályba sorolása. In *Műszaki Katonai Közlöny*, 2003, 13(1–4), 105–124.
- [5] HAJÓS B. Közúti hidak katonai és polgári terhelési osztályairól. In *Hadmérnök*, 2024, 19(2), pp. 49–62. Available at: <https://doi.org/10.32567/hm.2024.2.4>
- [6] HAJÓS, B. Movement of overload military and civil vehicles on road bridges. In *Katonai Logisztika 2024/1-2*, Budapest, pp. 230–247. Available at: <https://doi.org/10.30583/2024-1-2-230>
- [7] LENNER, R. *Safety Concept and Partial Factors for Military Assessment of Existing Concrete Bridges*. PhD Dissertation.

Universität der Bundeswehr München, Fakultät für Bauingenieurwesen und Umweltwissenschaften, 2014.

- [8] MSZ EN 1990:2011 Eurocode: A tartószerkezetek tervezésének alapjai. Basis of structural design.
- [9] EVERITT, A. 2019. *Dynamic load effects of tracked and wheeled military vehicles from bridge load testing*. A Thesis Submitted to the Division of Graduate Studies of the Royal Military College of Canada, MASc Thesis Document.
- [10] HORNBECK, B., KLUCK, J. and CONNOR, R. 2005. *Trilateral design and test code for military bridging and gap crossing equipment*. Report: Guide Specification, OMB No. 0704-0188. Available at: <https://doi.org/10.21236/ADA476104>
- [11] HAJÓS, B. A közúti hidak dinamikus tényezőjének csökkentési lehetőségei túlsúlyos civil járművek és nehéz katonai szállítások esetén. In *Útügyi lapok*, 2024(19). Available at: <https://doi.org/10.36246/UL.2024.1.03>

Dipl. Eng. Bence HAJÓS
Első Lánchíd Bt.
Bridge Engineer, Director
Nap utca 6.
4024 Debrecen
Hungary
E-mail: elsolanchid@elsolanchid.hu

Bence HAJÓS received a M.Sc. (Eng.) from the Budapest University of Technology and Economics (BME) in Hungary in 2001, in bridge engineering. Until 2014, he worked in the operation and maintenance of road and rail bridges. He is currently a private engineer, bridge inspection expert. His main research interests are bridge load capacity assessment, existing bridges, overload transports and bridge history. His research interests include the assessment of the military load capacity of existing road bridges in preparation for PhD degree at the Ludovica University of Public Service (Budapest).



MATERIALS AND TECHNOLOGIES IN THE DESIGN OF MILITARY OPTICAL DEVICES

Vratislav KREHEL, Michal MOZOLA, Martin KŘEPSKÝ

Abstract: Modern technologies offer promising possibilities in the design of optical devices through the use of advanced materials. These materials enable modifications of certain parameters, such as size, weight, and imaging properties, while also reducing costs by utilizing more affordable materials and lower-cost production methods. This article provides an analysis of the properties required to ensure the desired imaging quality, along with an overview of current and prospective modern materials suitable for constructing the bodies of optical devices.

Keywords: Design; Optical device; Invar; Aluminum; Polyethylene; Imaging errors; Temperature effects.

1 INTRODUCTION

Optical devices are designed to convert information from the observation (detection), measurement, or control of an object.

The fundamental components of optical instruments, including aiming telescopes, are all the parts that the designer must consider and that affect its properties. The basic building blocks include:

- a) **Imaging elements** – these create an image of the objects in the desired position, size, and quality.
- b) **Auxiliary elements** – these affect the position or orientation of the image but do not have a direct impact on its parameters. The optical tube of the instrument is classified as an auxiliary element. From this characterization, it might seem like a less important part of the device, but the opposite is true. In fact, the tube and all parts responsible for ensuring the correct positioning of the imaging elements have a significant impact on image quality.

Among the basic requirements we can include:

- **Sufficient strength and material durability** – the tube of a targeting telescope must ensure the stability of the optical elements' position even under shocks caused by recoil from a shot or during rough handling in combat operations.
- **Minimal thermal expansion** – ensure the correct positioning of the optical elements (objective lens, collector lens, reversing system, focal plate, and eyepiece) even with changes in the ambient temperature in which the optical instrument is used.

In the construction of a targeting telescope, the quality of the image is influenced by the appropriate selection of structural components of the telescope body, focal lengths, and the precision of mounting the optical parts, such as the objective lens, reversing system, and eyepiece [1].

The accuracy of aiming with a telescope will be influenced not only by the aforementioned construction parameters but also by changes

in temperature and atmospheric turbulence. Temperature, as an external factor, affects the size of the optical system. This leads to thermal expansion of the dimensions of the structural components as well as thermal optical aberrations of the objective lens. This can be mitigated in the design of the telescope through careful selection of materials and the structural arrangement of the optical system. It is essential to ensure that the construction materials have minimal sensitivity to temperature changes and that these thermal variations are mutually compensated [1].

Atmospheric turbulence causes changes in the angles of incidence of rays on the entrance pupil of the telescope's objective lens $\Delta\beta$. This disrupts the relationships between various parameters in the construction of optical elements. However, these effects cannot be completely eliminated by technical means [1].

2 ERRORS IN THE IMAGE OF AN OPTICAL SIGHT DUE TO TEMPERATURE AND ITS VARIATIONS

With changes in temperature of the telescope's structural components, there will be a change in their dimensions. If we assume that the temperature change affects only the length of the telescope body and does not impact the optical axis [1].

The deviation in the power of the telescope caused by changes in individual parameters is given by the relationship:

$$dK = \sqrt{\left(\frac{\partial K}{\partial \rho}\right)^2 \cdot \Delta\rho^2 + \left(\frac{\partial K}{\partial f}\right)^2 \cdot \Delta f^2} \quad (1)$$

where K is the magnification of the telescope, ρ is the resolving power of the device, and f the focal length of the objective lens.

After adjustment, we obtain the relationship for the deviation in the structural dimensions of the body and the focal lengths of the objective lens:

$$dK = K \cdot \sqrt{\frac{\Delta f^2}{f^4}} \quad (2)$$

If we vary the temperature of the sight body within the range $t \in \langle -20 \div 40 \rangle^\circ\text{C}$ and the coefficient of expansion $\alpha = 15 \cdot 10^{-6} \text{ m} \cdot ^\circ\text{C}^{-1}$. I will address this change in characteristics, which is significantly more complex, in the following text [1].

2.1 Thermo-optic aberrations of the objective lens and the position of the objective lens

A change in the temperature of the telescope will cause, in addition to structural changes in the body (tube) and optical system, alterations in the characteristics of image quality. These changes will be referred to as thermal aberrations in the following text [1].

Thermo-optic aberration of the image position is conditioned by:

- the dependence of the refractive index of the lenses on temperature,
- the change in the radius of curvature of the lens surfaces and the change in their thickness with temperature variations,
- the change in the distances between the lenses, which results from the thermal expansion of the telescope body material and the lens mounts [1].

In addressing thermo-optic aberrations and their impact on image quality, I will work with steady states. This means that the entire system is at the same temperature at the time of measurement [1].

If we consider that the coefficient of linear expansion of glass is temperature-dependent, it can be assumed that within certain precisely defined temperature change intervals, we can work with its average value. To correct the monochromatic aberration of the objective lens, we need to have a precisely defined wavelength of light for which we will analyze the aberration, as the thermal increment in the refractive index of light $\frac{dn}{dt}$ is dependent on this wavelength λ [1].

In designing an optical system that does not misalign with temperature changes, this can be achieved by selecting special types of materials for the lenses, lens mounts, and the body, to prevent changes in focal lengths and the occurrence of optical aberrations [1].

For an optical system consisting of optical surfaces, the optical aberration of the image position due to a change in temperature is given by the relationship:

$$ds'_k = \frac{n_1 \cdot h_1^2 \cdot s_k^2}{n_k \cdot h_k^2 \cdot s_1^2} \cdot ds_1 - \frac{h_1^2 \cdot s_k^2}{n_k \cdot h_k^2} \cdot T_1 \quad (3)$$

where s' is the image position [m], h is the distance from the target to the objective lens [m], n is the

number of refracting surfaces, and T_1 is the coefficient of thermo-optic aberration of the image position. The relationship for this coefficient is given by:

$$T_1 = \sum_{i=1}^k \frac{h_i^2}{h_1^2} \cdot \left[Q_{s,i} \cdot \left(\frac{dn_i}{n_i} - \frac{dn_i}{n_i} \right) \cdot (n_i - n_i) \cdot \frac{dr_i}{r_i^2} \right] + \sum_{i=2}^k \frac{h_i^2}{h_1^2} \cdot \frac{n_i}{s_i^2} \cdot dd_{i-1} \quad (4)$$

where Q_s is the zero invariant of the ray's refractive index on the surface:

$$Q_s = n \cdot \left(\frac{1}{r} - \frac{1}{s} \right) = n \cdot \left(\frac{1}{r} - \frac{1}{s} \right) \quad (5)$$

where r is the radius of the entrance pupil of the sight [m].

3 SELECTION OF MATERIAL FOR THE BODY OF A TARGETING TELESCOPE

In optical instruments, the material of the body and its properties are considered somewhat differently compared to mechanical engineering. Various materials with different properties, in terms of construction and processing methods, can be used. The emphasis is not primarily on the material's strength but rather on its machinability, dimensional stability, and shape stability.

All materials experience plastic deformation due to stress and especially due to heat. This is caused by flow and molecular instability of the material.

In mechanical engineering, flow is most commonly observed in components subjected to high temperatures, which occurs very infrequently in precision mechanics and optics. The manifestation of flow varies among materials. For example, it is minimal in fused quartz, while it is significant in zinc.

Internal stresses in a material arise either directly within the material itself or due to external influences. These stresses can occur during processes such as hardening. Annealing relieves these stresses, but not completely. Subsequently, flow may begin to manifest, and the component can continue to change its dimensions for years. For materials like duralumin, which is not annealed after thermal processing, these dimensional changes are significantly greater compared to steels.

Internal stresses also develop during cold processing, such as rolling and cold drawing. For example, in the drawing of a rod, the surface layer may experience compressive stresses, while tensile stresses occur inside the rod to maintain equilibrium. Reducing the diameter of the rod during machining removes some of the compressive stress [2].

Figure 1a shows that if a rod is machined symmetrically and the stress is also distributed symmetrically, the internal stress remains uniformly

distributed. The tensile stress inside the rod decreases, while the compressive stress on the surface increases, resulting in a shortening of the rod. Figure 1b and Figure 1c illustrate the asymmetric

distribution of stresses in the case of asymmetric machining and, conversely, symmetric machining if the stress distribution was asymmetric [2].

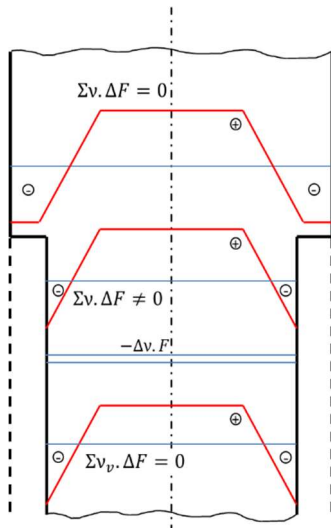


Fig. 1a Symmetrical distribution of internal stresses and symmetrical machining Source: [2].

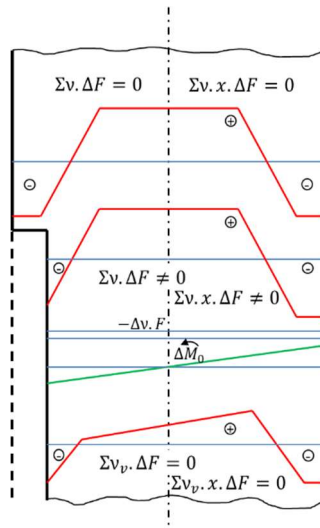


Fig. 1b Symmetrical distribution of internal stresses and asymmetric machining Source: [2].

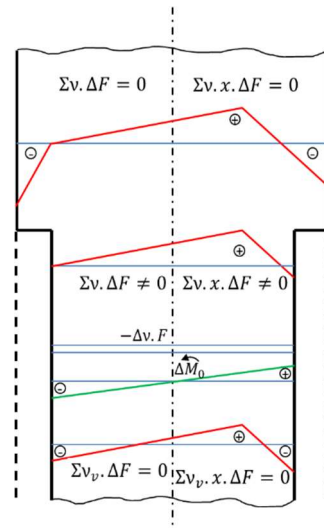


Fig. 1c Asymmetrical distribution of internal stresses and symmetrical machining Source: [2].

Dimensional and shape changes can be caused by molecular instability of the material, which may manifest spontaneously over the long term.

In precision mechanics and optics, the change in length due to temperature is also of significant importance. It can be approximately expressed by the equation:

$$\Delta L = L \cdot \alpha \cdot \theta \quad [mm] \quad (6)$$

where: **L** is the original length in mm;
α is the coefficient of thermal expansion;
θ = (**t₁** - **t₂**) is the temperature difference in °C.

The cause of a material's thermal properties is the thermal vibrations of atoms. At absolute zero (0K = -273,15°C), the atoms are in a stable position, and the atomic lattice has a zero equilibrium value. As the temperature increases, the atoms vibrate more and more, and at constant pressure, they move farther apart, which subsequently manifests as thermal expansion. This refers to the volumetric change **V** caused by an increase in temperature **T** at constant pressure **p** [2].

It can be expressed by the relationship:

$$\alpha = \frac{1}{V} \left(\frac{\partial V}{\partial T} \right)_p \quad (7)$$

For selecting materials for the body of a targeting telescope, I will focus on two commonly used materials in optics and one modern material. I will

compare these materials in terms of their response to temperature changes [3].

3.1 Invar

Invar (from the French "invariability") is an alloy of iron with 36 % nickel. It has the lowest thermal expansion among metals. It is silver-gray, corrosion-resistant, and a very poor conductor of heat and electricity. The coefficient of thermal expansion depends on the alloying elements, impurities, and both thermal and mechanical processing. There are several variants of Invar with coefficients of thermal expansion of 0.8, 1.0, 1.6, and 2,5.10⁻⁶. The instability of this material is manifested in temporal irregularity and thermal expansion, especially in slowly occurring length changes, which can appear over years. Complex long-term artificial aging processes do not help either. One method of stabilization is to place the Invar rod into a thin, long solenoid connected to the power supply for 48 hours, where the alternating current excites the molecules through alternating magnetization, causing alternating longitudinal changes due to magnetostriction (changes in material dimensions when magnetized), and also because the rod slightly heats up. More modern types of Invar, which are slightly alloyed with additional elements such as chromium, show more regular behavior. Adding cobalt as an alloying element can reduce the coefficient of thermal expansion of Invar at low temperatures (up to 100°C). This alloy is called Superinvar [2, 4].

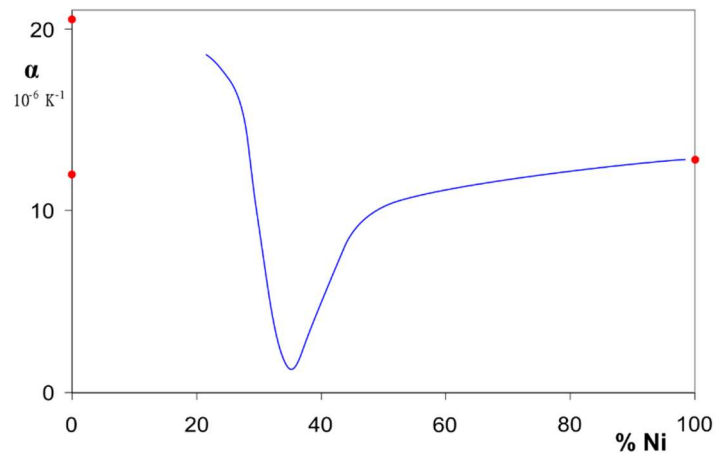


Fig. 2 The effect of nickel on changes in the coefficient of thermal expansion
Source: [5].

Tab. 1 Basic Properties of alloy FeNi36 – Invar

Density at 20°C	8100 kg./m ³
Melting temperature	1450°C
Coefficient of expansion at 20°C and 100°C	1,2 10 ⁻⁶ K ⁻¹
Hardness (HB)	220
Modulus of elasticity at 20°C	140 GPa
Yield strength	700 MPa
Tensile strength	750 MPa

Source: [6].

Applications of Invar:

Invar is used for applications requiring the lowest possible thermal expansion.

Most common uses [7]:

- Manufacturing, storage, and transportation of liquefied gases;
- Components for OLED displays;
- Measurement and control devices for temperatures below 200 °C (392 °F), such as thermostats;
- Casings for screw or rivet joints between different metals;
- Bimetallic components and thermostatic bimetals where Invar is the passive component;
- Molds for producing carbon fiber reinforced plastics (CFRP), especially in the aerospace industry;
- Structures for electronic control units in satellites and space equipment down to -200 °C (-328 °F);
- Support elements for electromagnetic lenses in laser control units;
- Flywheels;
- Automotive components;
- Transport of liquefied hydrogen;
- Optics and precision mechanics.

3.2 Aluminum

Aluminum oxide was discovered in the late 18th century, paving the way for aluminum production.

However, it wasn't until the mid-19th century that small quantities of aluminum were produced and methods for its industrial production were developed. These methods were initially too complex and economically demanding. Later, in 1886, Paul (Louis-Toussaint) Héroult and Charles Martin Hall independently developed the process of extracting aluminum through the electrolysis of aluminum oxide. This method, with minor modifications, remains in use today.

Aluminum is a lightweight, silvery-white metal. It can be drawn into wires, rolled into thin sheets, and made into foils. Pure aluminum is processed through extrusion, drawing, and stamping. In electrical engineering, aluminum is used as a conductor and as a surface protection for iron (through alloying and calozation). It resists corrosion, and anodizing (electrolytic oxidation) can enhance surface hardness. It is also used in precision mechanics, measuring instruments, and other applications. Aluminum is employed in mirrors designed to reflect short-wavelength ultraviolet rays, such as those used in astronomical telescopes for photographing the sky. This is achieved by creating a thin layer of aluminum through vacuum deposition of aluminum vapor [2, 8].

3.2.1 Aluminum Alloys

Aluminum alloys, in contrast to pure aluminum, have significantly better mechanical properties. This advantage is especially evident in aerospace

manufacturing, where aluminum alloys replace much heavier steel components [8].

The extensive development of alloy usage encompasses a wide variety of alloys based on chemical composition, application area, and processing methods [8].

Typically, aluminum alloys are divided into two main categories: wrought alloys and cast alloys. Both categories share common alloying elements. Some alloys lie at the boundary between these categories and can be used for both processing methods [8].

The basic binary aluminum alloys are Al-Cu, Al-Mg, Al-Mn, Al-Si, and Al-Zn. In these systems, aluminum forms a substitutional solid solution with the corresponding components, which is stronger and harder than pure aluminum while maintaining good formability and toughness [8].

This is reflected as follows:

Copper – increases the strength and hardness of the alloy but reduces its formability. In wrought alloys, copper typically makes up to 6 %, while in casting alloys, it can be up to 12 %. It adversely affects corrosion resistance [8].

Magnesium – appears in small amounts in almost all aluminum alloys. It primarily improves conditions for

heat treatment and enhances corrosion resistance. The magnesium content is typically 8 % in wrought alloys and 11 % in cast alloys [8].

Manganese – improves strength, ductility, and corrosion resistance. At higher concentrations, it increases brittleness and worsens castability [8].

Zinc – provides greater strength, reduced toughness, and improved corrosion resistance. Low ductility at room temperature improves at higher temperatures [8].

Iron and Silicon – are common additives in aluminum. In alloys for forging, the iron content is up to 0.5 %, and in special cases, up to 1.6 %. In casting alloys, iron additions up to 1 % improve properties. Silicon content varies; casting alloys may contain up to 13 %, and in some cases, up to 25 % [8].

Nickel – increases mechanical properties at both normal and elevated temperatures and improves corrosion resistance [8].

Other elements such as chromium, cobalt, tungsten, titanium, vanadium, and zirconium, among others, positively influence the refinement of crystallization even in very small quantities. This is essentially the main reason for the use of these elements in aluminum alloys [8].

Tab. 2 Chemical Composition of Some Aluminum Alloys

Aluminum sheets and plates and their weight percentage of alloying elements (%)

ALUMINUM ALLOY	Si	Fe	Cu	Mn	Mg	Cr	Zn	Ti	OSTATNÉ
EN AW 1050 A	0,25	0,4	0,05	0,01	-	0,01	0,07	0,05	0,03
EN AW 2017 A	0,20 - 0,80	0,7	3,50 - 4,50	0,40 - 1,00	-	0,10	0,25	0,25	0,15
EN AW 5005 A	0,20 - 0,80	0,7	3,50 - 4,50	0,40 - 1,00	-	0,10	0,25	-	0,15
EN AW 5083	0,40	0,4	0,10	0,40 - 0,10	4,00 - 4,90	0,05 - 0,25	0,25	-	0,35
EN AW 5754	0,40	0,4	0,10	0,50	2,60 - 3,60	0,30	0,20	0,40	0,40
EN AW 6082	0,70 - 1,30	0,5	0,10	0,40 - 1,00	2,60 - 1,20	0,25	0,20	-	0,30
EN AW 7075	0,40	0,5	1,20 - 2,00	0,30	2,10 - 2,90	0,18 - 0,28	5,10 - 6,10	0,20	0,15
EN AC 5083	0,40	0,40,10		0,40 - 1,00	4,00 - 4,90	0,05 - 0,25	0,25	-	0,15

* Aluminum and common impurities make up the remainder

Source: [9].

Tab. 3 Basic Properties of alloy EN AW 5083

Density at 20°C	2660 kg./m ³
Melting temperature	575-638°C
Coefficient of expansion at 20°C and 100°C	24,2 10 ⁻⁶ K ⁻¹
Hardness (HB)	Not specified
Modulus of elasticity at 20°C	70 GPa
Yield strength	110 MPa
Tensile strength	270 MPa

Source: [10].

Applications EN AW 5083

Most common applications [11]:

- Machinery: shipbuilding, welded structures, precision parts, molds, medium-load components, foaming molds, vehicle production.
- Construction: components where high corrosion resistance and medium strength are required.
- Chemical industry: tanks and parts where high corrosion resistance and medium strength are required.

- **PEX** (Cross-Linked PE):
Cross-linked polyethylene
- **MDPE** (Medium Density PE):
Medium-density polyethylene
- **LDPE** (Low Density PE):
Low-density polyethylene
- **LLDPE** (Linear Low Density PE):
Linear low-density polyethylene
- **VLDPE** (Very Low Density PE):
Very low-density polyethylene [12]

3.3 Polyethylene (PE) and its Modifications

Polyethylene (PE), chemically known as poly(ethylene), is a thermoplastic polymer used in numerous technical applications. The annual production of PE reaches 60.10⁹ kg. It is manufactured through the polymerization of ethylene. Various polymerization methods can be employed: radical polymerization, anionic or cationic addition polymerization, and ionic coordination polymerization. Each of these methods results in PE with different physical and mechanical properties [12].

Polyethylene (PE) is classified into several categories, primarily differing in terms of molecular weight, degree of chain branching, and density, which reflect their physical-mechanical properties [12].

Basic Classification:

- **UHMWPE** (Ultra High Molecular Weight PE):
Ultra-high molecular weight polyethylene
- **HMWPE** (High Molecular Weight PE):
High molecular weight polyethylene
- **HDPE** (High Density PE):
High-density polyethylene
- **HDXLPE** (High Density Cross-Linked PE):
Cross-linked high-density polyethylene

By comparing the properties of the mentioned polyethylene modifications, UHMWPE (Ultra High Molecular Weight Polyethylene) appears to be the best option for constructing a telescope, as it can also be used for the tube. This polymer has extremely long polymer chains with high molecular weight. The molecular weight of these chains and their low branching allow for very good chain packing into crystalline structures. As a result, UHMWPE is a very strong and tough material with the highest impact toughness among thermoplastics. UHMWPE exhibits excellent resistance to corrosive chemicals, except for oxidative acids. It has extremely low moisture absorption, a very low coefficient of friction, is self-lubricating, and highly resistant to abrasion (up to 10 times more resistant compared to carbon steel) [12].

The advantages of UHMWPE include excellent strength, toughness, and resistance to abrasion and chemicals. The disadvantage is that UHMWPE cannot be processed by melting, as thermal decomposition occurs before the polymer melts [12].

Applications of UHMWPE include fibers and textiles (fishing nets, bulletproof vests), bearings, gears and drives, artificial joints, moving parts of spinning and weaving machines, various protective strips, butcher's blocks, lining for chutes and slides for abrasive materials, and more [12].

Tab. 4 Properties of UHMWPE

Polyethylene (PE) UHMWPE

Density:	934 - 980 kg/m ³		
Crystallinity:	> 90 %		
Water absorption:	0,01 %		
Mechanical properties		Physical properties	
Young's modulus of elasticity:	0,7 GPa	Max. service temperature:	155 °C
Modulus of elasticity in bending:	0,75 GPa	Thermal conductivity:	0,403 - 0,435 W/m.K
Tensile strength:	35 - 40 MPa	Specific heat capacity:	1,8 - 1,88 kJ/kg.K
Yield strength:	18 - 29 MPa	Coefficient of thermal expansion:	125 - 200 .10 ⁻⁶ .K ⁻¹
Elongation:	300 - 850 %	Flammability UL94:	HB
Extension at yield point:	25 %	Oxygen index:	17 %
Hardness (Rockwell R):	50	Electrical resistivity:	10 ¹⁸ Ω.cm
Fracture toughness:	1,4 - 1,7 MPa.m ^{1/2}	Breakdown voltage:	28 MV/m
		Dielectric constant:	2,3
		Dissipation factor:	0,0002

Source: [13].

Applications UHMWPE

The most common uses [14]:

Bearings: Wear-resistant profiles and segments, chain guides.

Conveyor: conveyor elements, conveyor chutes, sliding conveyor liners, conveyor star wheels, antistatic sliding components, curved tracks, arcuate guides, conveyor belts.

Sliding elements: sliding rails, sliding profiles, sliding segments.

Other applications: scraper blades, containers, outlets, belt insulation, seals, guiding elements, sliding components, plain bearings, connecting belts, sliding parts with high wear resistance, chain guides, gears, crane foot support plates, bearing sleeves, pressing belts, pump components, belt guides, rollers for roller tracks, chain conveyors, conveyor chutes, deflection rollers, guiding rails, and workpiece carriers on conveyors [14].

4 CONCLUSION

In the environmental analysis, we must consider the changes in the parameters of the lenses, which result from variations in temperature and pressure. Such an affected system becomes the foundation for evaluating image quality. When monitoring changes in optical properties, we take into account the initial conditions:

- Nominal temperature of 20 °C;
- All spaces, including the object and image spaces, are filled with air under a pressure of 1013.25×10^9 Pa (sea level pressure);
- The refractive index of air is considered to be 1.0, which is the assumption stated in optical glass catalogs [15].

Any change in temperature will cause all glass elements to expand or contract according to the coefficient of thermal expansion. This will affect the radius of curvature, axial thickness, aperture radius, and aspheric coefficients according to the following relationship:

$$L(T + \Delta T) = (1 + \alpha \cdot \Delta T) \cdot L_0 \quad (8)$$

where L is the length at the changed temperature, T is the reference temperature, ΔT is the temperature change, and α is the coefficient of linear expansion. All spaces filled with air will change due to heat according to the axial thicknesses, summing the individual thickness changes. If strongly curved surfaces are used in the optical system, the length of the spacers may significantly differ from the axial air space.

4.1 Assessment of the Impact of Heat on the Design of the Optical System

To meet certain thermal performance requirements of the optical system, such as athermalization, it is sometimes necessary to use special mounting techniques, where individual lenses or groups of lenses are secured in separate housings. Materials with abnormal coefficients of thermal expansion are often used for these housings in order to maintain image focus without any focusing mechanism (so-called passive athermalization) [15].

With temperature changes, lenses or even entire lens groups may shift relative to other surfaces, typically different from the immediately preceding one. As a result, the space between two lenses changes, which is not dependent on the thermal expansion coefficient of the housing material but rather on a more complex principle [15].

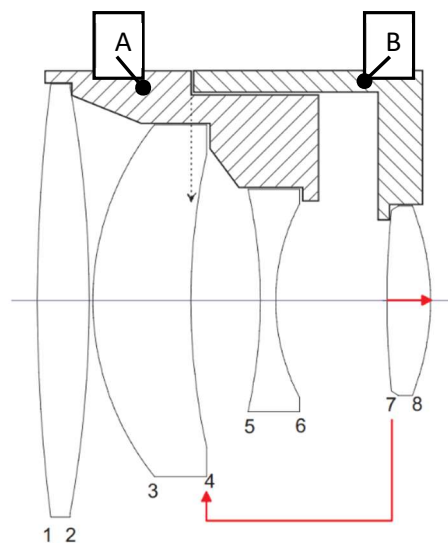


Fig. 3 The Effect of Thermal Expansion on Global Reference Surfaces
Source: [15].

In Figure 3, a simple optical system is illustrated where the final lens of the system, with surfaces 7-8, is mounted in a separate housing **B** attached to a flange on the main housing **A** at the surface 4 of the second lens. If the main and secondary housings were made from different materials, the space between the third and fourth lenses would vary according to the difference in thermal expansion of these two materials [15].

Given these considerations, it is crucial to focus on the appropriate selection of materials for optical instruments. The most important factor is to choose an optimal material for optical elements so that thermal effects minimally impact image quality. Subsequently, it is essential to select a tube or housing material for the optical system that either minimizes the resulting changes or compensates for them through the beneficial effects of thermal expansion of the material.

4.2 Comparison of the Thermal Expansion of Selected Materials

After examining the properties of the materials discussed in the paper and considering them as the most promising for the construction of the targeting telescope body, and subsequently comparing the material data sheets and cited sources, I can conclude the following:

The coefficient of thermal expansion is the most important parameter that has the greatest impact on the quality and accuracy of imaging in optical systems.

The materials have the following coefficients of thermal expansion:

Invar alloy FeNi36	$1,2 \cdot 10^{-6} \text{ K}^{-1}$
Aluminum alloy EN AW 5083	$24,2 \cdot 10^{-6} \text{ K}^{-1}$
Polyethylene (PE) UHMWPE	$125 - 200 \cdot 10^{-6} \text{ K}^{-1}$

From this, it follows that the material with the lowest coefficient of thermal expansion, relative to the same coefficient of expansion of the glass used in the optical system, is the most suitable. In this case, Invar is the most frequently used material in optical systems due to this physical property. However, since the optical systems of targeting telescopes are complex assemblies of several lens groups, other materials can be considered as compensatory elements for passive athermalization.

References

[1] BALÁŽ, T. *Possibilities for Utilizing Passive Optoelectronic Rangefinders in Contemporary Tank and Armored Fighting Vehicle Fire Control Systems*. Brno, 2003.

[2] KAMARAD, J. *Basic Qualification Textbook Precision Mechanics and Optics*. Praha, 1974.

[3] PÍŠEK, F. *Materials Science I: Metals Volume 2*. Praha, 1968.

[4] PÍŠEK, F. *Materials Science I: Metals Volume 4*. Praha, 1975.

[5] INVAR. [cit. 2024-09-16]. Available at: <https://en.wikipedia.org/wiki/Invar>

[6] *Material data sheet of the alloy FeNi36*. [cit. 2024-09-16]. Available at: <http://www.koro.cz/static/useruploads/files/nikl-cz/FeNi36-pasy.pdf>

[7] *VDM® Alloy 36*. [cit. 2024-09-16]. Available at: https://www.vdm-metals.com/fileadmin/user_upload/Downloads/Data_Sheets/Data_Sheet_VDM_Alloy_36.pdf

[8] PÍŠEK, F. *Materials Science I: Metals Volume 3*. Praha, 1973.

[9] *Properties and standards of aluminum alloys*. [cit. 2024-09-16]. Available at: <https://www.hlinik.sk/vlastnosti-a-normy-hlinikovych-zliatin/>

[10] *Material data sheet of the alloy EN AW 5083 ČSN 424415*. [cit. 2024-06-20]. Available at: <https://www.nedal.com/wp-content/uploads/2017/11/Nedal-alloy-Datasheet-EN-AW-5083.pdf>

[11] *Applications of aluminum alloys*. [cit. 2024-09-16]. Available at: <https://www.hlinik.sk/vyuzitie-zliatin/>

[12] *Polyethylene (PE)*. [cit. 2022-06-20]. Available at: <http://www.matnet.sav.sk/index.php?ID=504>

[13] *Polyethylene (PE) UHMWPE. Properties*. [cit. 2022-06-20]. Available at: <http://www.matnet.sav.sk/data/files/795.pdf>

[14] *Murdotec® 2000 natural, our UHMW-PE*. [cit. 2022-06-27]. Available at: https://matmatch.com/materials/murd0016-murdotec-2000-natural?utm_term=pe%20uhmw%20material&utm_medium=ppc&utm_campaign=%5BSN%5D%5BCS%5D+Murdotec&utm_source=adwords&hsa_grp=116297599343&hsa_cam=12317907011&hsa_src=g&hsa_net=adwords&hsa_tgt=kwd-550940086936&hsa_ad=505193782949&hsa_mt=b&hsa_kw=pe%20uhmw%20material&hsa_ver=3&hsa_acc=2813184419&gclid=CjwKC_AjwquWVBhBrEiwAt1Kmwjbf0j4YtPYOrCTB5EzopIMJ0DJuYNakFphSzN2Lhd0yzzpE9bgjDBoCUxgQAvD_BwE

[15] *OpTaliX, Software for Optical Design and Thin Films*. Reference Manual, Version 6.98, Heerbrugg, 2008.

[16] TRAEGER, F. *Springer Handbook of Lasers and Optics*. Berlin, 2012. Available at: <https://doi.org/10.1007/978-3-642-19409-2>

[17] MADOU, M. *Fundamentals of Microfabrication and Nanotechnology*. Boca

Raton, USA, 2018. Available at:

<https://doi.org/10.1201/9781315274164>

- [18] SHACKELFORD, J. F. *Introduction to Materials Science for Engineers*. Boston, USA, 2015.
- [19] LI, J. C. M.. *Metals and Alloys: Industrial Applications*. Cham, 2019.
- [20] SINGH, J. *Optical Properties of Materials and Their Applications*. Chichester. UK, 2020.
- [21] *Advanced Optical Materials*, Wiley-VCH, Weinheim, 2021.

Martin KŘEPSKÝ was born in 1980, is absolvent of Military Academy in Brno (2003) and University of Pardubice (2021). After the graduation from Military Academy he has been assigned to different command and training posts of the Armed Forces of the Czech Republic. His interest is in optoelectronic means of detection and identification of chemical agents.

Dipl. Eng. Vratislav **KREHEL**

Armed Forces Academy of General M. R. Štefánik
Demänová 393
031 01 Liptovský Mikuláš
Slovak Republic
E-mail: vratislav.krehel@aos.sk

Capt. Dipl. Eng. Michal **MOZOĽA**

Armed Forces Academy of General M. R. Štefánik
Demänová 393
031 01 Liptovský Mikuláš
Slovak Republic
E-mail: michal.mozola@aos.sk

Maj. Dipl. Eng. Martin **KŘEPSKÝ**

JCBRN Defence COE
Víta Nejedlého
682 01 Vyškov
Czech Republic
E-mail: martin.krepsky@unob.cz

Vratislav KREHEL was born in Liptovský Mikuláš, Slovakia in 1972. He received his M. Sc (Eng.) at the Military Academy in Liptovský Mikuláš in 2003. He started his dissertation studies in 2021. His research interests are focused on optimization of sniper weapons fire mode. He is currently working as an assistant professor at the Department of Mechanical Engineering, Armed Forces Academy of General M. R. Štefánik in Liptovský Mikuláš.

Michal MOZOĽA was born in Krupina, Slovakia in 1988. He received his M. Sc (Eng.) at the Armed Forces Academy in Liptovský Mikuláš in 2017. He started his dissertation studies in 2022. His research interests are focused on the optimisation of automatic weapon fire modes. He is currently working as an assistant professor at the Department of Mechanical Engineering, Armed Forces Academy of General M. R. Štefánik in Liptovský Mikuláš.



INFLUENCE OF BULLET SHAPE ON .223 REMINGTON AMMUNITION ACCURACY ANALYSIS

Tomáš RÁZGA, Peter BALÁŽ, Michal MOZOLA, Vratislav KREHEĽ

Abstract: The quality of ammunition significantly affects the accuracy of small-caliber weapons. Many articles emphasize the importance of well-made ammunition. There is a wide variety of .223 Remington ammunition available from local manufacturers, often with a typical 55-grain bullet weight but different bullet shapes. This article discusses the measured results of different bullet shape dispersions and possible causes of these adverse events.

Keywords: Bullet shape; Accuracy; Ammunition; Powder charge.

1 INTRODUCTION

The quality of ammunition is as important as the quality of the weapons that soldiers use. Since the 1960s, 5.56x45 mm ammunition, known in civilian circles as .223 Remington, has been very popular. The differences between these two are small, but can have a large impact on performance, safety, and weapon function.

The first one is the higher pressure level of the 5.56 NATO cartridge, which can approximately jump up to 450 MPa. The .223 Remington's maximum pressure load is approximately 430 Mpa. The second one and the most important difference is that a 5.56 NATO chamber has a .125" longer throat. This allows one more grain of powder to add into a 5.56 NATO cartridge, giving it higher performance than its .223 Remington counterpart.

The most significant issue with these differences is during firing with a rifle chambered for .223 Remington with 5.56 NATO ammunition. Due to the longer throat of the NATO chamber, this combination will cause the pressure increase at approximately 450 MPa or more the .223 chambered weapon, which is 50 MPa higher than the .223's normal functional pressure of 400 MPa. This is not safe and can cause primers to back out or worse, can harm the operator, the rifle, or both.

Conversely, firing a .223 Remington cartridge in a 5.56 NATO chambered rifle can result in suboptimal performance due to the throat difference. The .223 Remington's 380 MPa will not be attained, thus hurting velocity and performance. Problems start occurring when this combination is fired out of a 5.56 NATO chambered rifle with a 14.5" (or shorter) barrel. The lower powder charge of the .223 round, coupled with the pressure drop in the 5.56 NATO chamber, will cause the rifle to cycle improperly. NATO chambered rifles with barrels longer than 14.5" should function properly when firing .223 Rem ammunition.

The .223 Remington is one of the most common rounds in the world. It is very versatile and popular

for hunting, military, and sport shooting. The typical bullet weight ranges from 40 to 90 grains, depending on the weapon twist.

Tab. 1 Parameters of .223 Remington round with 55grs bullet

Type of brass	Rimless
The bullet diameter (mm)	5,7
The neck diameter (mm)	6,4
The brass thick (mm)	1,1
The crimp diameter (mm)	9,0
The brass length (mm)	45
The maximum pressure (MPa)	430
The maximum overall length (mm)	57,4
The type of primer	Boxer

Source: authors.

The good modern rifle should make dispersion closer to 1 MOA (Minute of angle), which means that dispersion of shots is smaller than 29mm at 100m. For example soviet era made SVD Dragunov should have efficiency 1,5 MOA with 7,62x54 mm round.

A lot of sport shooters and hunters made their own ammunition. This kind of process is known as a reloading. They can make more quality rounds than mass industry.

A lot manufactros made typical .223 Remington 55 grs weight bullets but bullets have different shape. When we read reloading manual a we want to use some kind of gunpowder, we always find how many of gunpowder we should use to bullet of some weight. Based on this is shape of bullet not as important as a weight of bullet.

2 THE EFFECTS OF RIFLE BULLET SHAPE

Looking back at the history of projectiles, the earliest jacketed bullets were round-nosed,

reminiscent of the lead bullet designs from the mid to late 19th century.

At moderate ranges, these bullets provided everything hunters and shooters needed: adequate accuracy, a weight-forward design that improved straight-line penetration, and a compact length-to-width ratio that fit efficiently in the cartridge case.

As the 20th century approached, and particularly following the Spanish-American War, the U.S. Army decided to update its .30-40 Krag cartridge, opting for the .30-03, which retained the Krag's 220-grain round-nose bullet. However, within just three years, the U.S. followed the example of European designers by modifying the '03 case and adopting a lighter, pointed spitzer bullet. A boat tail - almost as important as the pointed tip - was introduced to enhance the bullet's aerodynamic properties at longer ranges, resulting in a flatter trajectory and better retained velocities as distance increased.

Interestingly, the boat tail design had appeared as early as 1901, illustrating the rapid advancements in ballistic science. Fast forward to 2020, and you'll find all these designs still available and performing well, each for its unique advantages. Let's explore the benefits and drawbacks of these different rifle bullet designs to help guide your decision-making process.

2.1 The roundnose bullets

Round-nose bullets remain a popular choice among classic cartridge enthusiasts and can still be effective for hunting, as long as the shooting distances aren't too great. For this discussion, I'll also include flat-nose bullets, as their performance is quite similar.

The main limitation of round-nose bullets is their low ballistic coefficient (BC) - which measures how efficiently they travel through the air. This lower BC causes their velocity to drop off significantly beyond 200 meters.

2.2 The spitzer design

When we shift to the spitzer design, there's a clear advantage in trajectory, especially for longer shots. Boat tail spitzers, particularly modern iterations, are marvels of design, with an incredible amount of science behind them - nearly perfecting the projectile. Both target and hunting bullets fall into this category, making them a top choice for those hunting in open plains or mountainous regions where windy conditions can be a significant challenge. For long-range precision shooters - those who hit targets beyond 1,000 yards and sometimes even past a mile - this bullet profile is indispensable, as no other design offers the same level of performance at extended distances.

For target shooters, the discussion almost always centers around the boat tail spitzer. These bullets boast the highest ballistic coefficient values, making them the go-to choice. However, it's worth noting

that in cup-and-core designs, they can be susceptible to jacket and core separation.

3 THE EXPERIMENT

For the practical experiment we use numerous types of bullets and rounds. The mass industry is represented by FIOCCHI .223 Remington FMJ. As the name suggest the bullet is full metal jacket round without boat tail. The weight of the bullet is 55grs.

Tab. 2 Parameters of FIOCCHI .223 Remington round with 55grs bullet

The type of the bullet	FMJ
The weight of the bullet (grs)	55
Muzzle velocity (m/s)	980
Muzzle energy (j)	1711
Bullet path at 100m (cm)	0
Bullet path at 200m (cm)	-8
Bullet path at 300m (cm)	-35
Bullet path at 400m (cm)	-87
Ballistic coefficient G1(lb/in ²)	0,195

Source: authors.



Fig. 1 FIOCCHI .223 Remington round with 55grs bullet
Source: authors.

3.1 The reloading of own rounds

For the practical experiment we also used 4 types of 55 grs bullets:

- .224 RN 55grs from H&N Sport;
- .224 SP 55grs from Sellier & Bellot;
- .224 FMJ 55 grs from Sellier & Bellot;
- .224 Blitzking 55 grs from Sierra.

RN means round nose bullets. These are typically pistol bullets with a semi circular nose. They can also be found in rifle calibers, but this is more rare. This RN bullets have flat-base design.

FMJ means full metal jacket bullets. Similar to FMJ are SP bullets, soft point. Soft-point bullets offer more expansion than a full metal jacket bullet and greater penetration than a hollow point. A soft-point bullet is essentially a full metal jacket bullet, which has a lead core wrapped in a hard copper casing, with the lead tip exposed at the nose of the bullet. To make a full metal jacket, the copper shell or “cup” of the bullet is made with an opening at the bottom, allowing lead to be poured inside. Because of the manufacturing process, full metal jackets usually have exposed lead at the rear. Both, SP and FMJ are not totally sharp. FMJ bullets have boat tail and SP bullets have flat-base.

According Sierra company, the Blitzking type of bullet should be one of the most accurate bullet types. The nose tips of bullets are made of a proprietary acetyl resin compound, and the sharp tips improve the ballistic coefficient over the traditional flat-base Spitzer bullet design. The 55 grain has a boat tail to further increase ballistic coefficient compared to a flat-base design in these bullet weights.



Fig. 2 Types of bullets which were use in experiment.
From left to right: RN type, FMJ type, SP type and Blitzking design
Source: authors.



Fig. 3 .224 RN 55grs from H&N Sports
Source: authors.



Fig. 4 .224 SP 55grs from Sellier & Bellot
Source: authors.



Fig. 5 .224 FMJ 55grs from Sierra
Source: authors.



Fig. 6 .224 FMJ 55grs from Sierra
Source: authors.

For laboration we used single operation press LEE Precision Breech Lock Challenge Press. We use onetime shot brasses, which all of them were from Sellier & Bellot company. All cartridge cases were cleaned a reformed by Full length sizer die. We also cleaned the neck of cartridge and his primer seat. As a new primer were used 4,4 mm Small pistol primers from FIOCCHI Company. We have a lot of good experimencies with this primer manufacor. Primers are reliable and very suitable for .223 remington rounds despide that they are made for pistols and revolvers. .223 Remington is rifle round

but there is not a big pressure and due to that we are not force to use rifle primers, which are a little stronger than pistol one.

After that we set new primer. Primer was manufactured by FIOCCHI and it was Small pistol 4,4 mm. We used LOVEX D-073,4-03 gunpowder. According loading manual we used 1,60 g of gunpowder for each round.



Fig. 7 4,4 mm Small pistol primers used in our rounds
Source: authors.



Fig. 8 LEE Precision Breech Lock Challenge Press
Source: authors.

All cartridge cases were adjusted by Lyman Case Prep Xpress for the exact case length. There were cleaned and prepared primer seat and case neck for setting a bullet. All cartridge cases had similar length.



Fig. 9 Lyman Case Prep Xpress
Source: <https://www.amazon.ca/Lyman-Case-Prep-Xpress-115-Volt/dp/B004TABTWU>



Fig. 10 Cleaning primer seat at Lyman machine
Source: <https://www.amazon.ca/Lyman-Case-Prep-Xpress-115-Volt/dp/B004TABTWU>



Fig. 11 The lubrication and cleaning case neck
Source: <https://www.amazon.ca/Lyman-Case-Prep-Xpress-115-Volt/dp/B004TABTWU>



Fig. 12 The adapting case neck for seating a bullet
Source: <https://www.amazon.ca/Lyman-Case-Prep-Xpress-115-Volt/dp/B004TABTWU>

D-073,4 is two-component dense spheric gunpowder, which is one of the most popular gunpowder for reloading .223 Remington ammunition in the world. In contrast with pistol gunpowder, grains of this powder has different shape and burning rate is not as fast as spherically powder.



Fig. 13 D-073,4 gunpowder
Source: authors.



Fig. 14 D-073,4 gunpowder
Source: authors.



Fig. 15 The most popular gunpowders and their grains
Source: authors.

3.2 THE SHOOTING TEST

For shooting part was used AR-15 base rifle PAR Mk-3. We were shooting at open air shooting range situated in Liptovské Sliache area. The shooting conditions were favorable, with a temperature of 5 degrees Celsius and minimal wind interference. The cool temperature provided stable air density, contributing to consistent bullet trajectory. Visibility was clear, and overall conditions allowed for precise testing without significant environmental factors affecting the results. We were shooting at distance of 100 metres, due to fact, that we want to calcute accuracy in MOAs. Shooter (author) was shooting from the prone position and used bipod. We wanted to get close to combat conditions and due that fact,

we did not use stative stand. If we consider possibilities of shooter's errors, we selected from this experiment one best series consisting of the best 5 shots, from the total number 15 shots.

Each of the shots was shot through the chronometer what is a machine, which calculate speed of the bullet. The fact, that gas escaping from the muzzle and it may affects our results, the chronometer was 1m away from the rifle of the muzzle.

At next series of pictures we could see impact of bullet shape on hit dispersion (yellow circle). As we could see there is a notable difference between hits (red circles), mainly between aiming point (green cross) and middle hit (yellow cross).

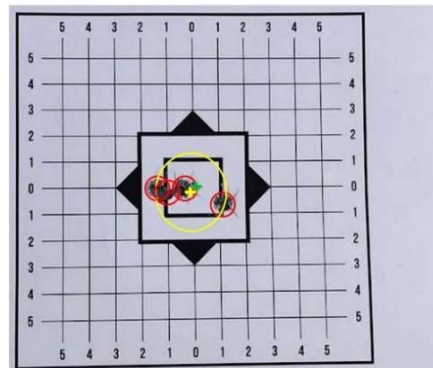


Fig. 16 Accuracy of Blitzking bullets
Source: author.

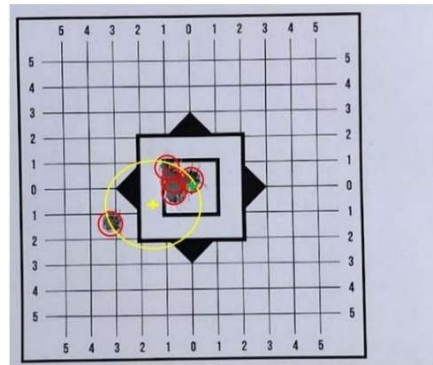


Fig. 17 Accuracy of FIOCCHI factory 223 Remington rounds
Source: authors.

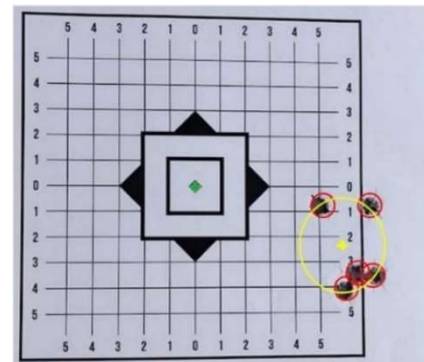


Fig. 18 Accuracy of FMJ bullets
Source: authors.

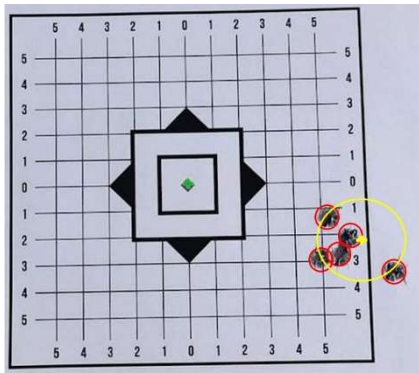


Fig. 19 Accuracy of SP bullets
Source: authors.

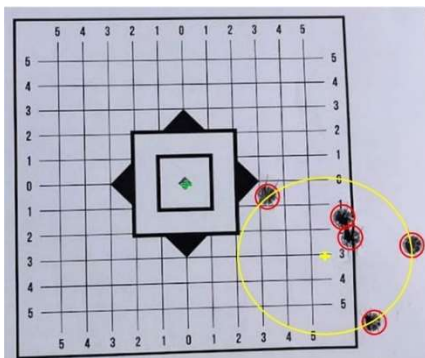


Fig. 20 Accuracy of RN bullets
Source: authors.

As we can see there are important differences in accuracy between each series. The best result was made with Blitzking bullets. The rounds, which do not have on bullet boat tail, had significant worse dispersion and position of middle hit was displaced to the right down side.

This is due to fact, that rifle has 1:8 right turn twist rate and 16 inch barrel. Rounds with SP and RN bullets have smaller muzzle velocity and stabilization did not work properly. Another thing which had impact was that, SP and RN bullets are shorter and do not have exact aerodynamical shape.

Tab. 3 Parameters of FIOCCHI .223 Remington round with 55grs bullet

Bullet	Dispersion (diameter in mm)	Distance between middle hit and aiming point (mm)
RN	69	68
FMJ	35,5	
FMJ FIOCCHI	37	17
SP	32,5	62,5
BLITZKING	27,5	4

Source: authors.

Tab. 4 Muzzle velocity

Bullet	Muzzle velocity (m/s)
RN	880
FMJ	923
FMJ FIOCCHI	973
SP	940
BLITZKING	955

Source: authors.

Statistical analysis was conducted to evaluate the significance of the differences observed. The mean dispersion (in cm) and standard deviation for each type of bullet are presented in Table 3.

Tab. 5 Mean dispersion

Bullet type	Mean Dispersion (cm)	Standard Deviation (cm)	Muzzle velocity (m/s)
FMJ	2,3	0,5	880
HP	3,1	0,7	923
SP	4,2	1,0	973

Source: author.

The mean dispersion for each bullet type was calculated using the formula:

$$\bar{x} = \frac{1}{n} \sum_{i=1}^n x_i \tag{1}$$

where n is the number of measurements and x_i are the individual dispersion values.

Based on the experimental results, the mean dispersion and standard deviation for each bullet type were calculated. The standard deviation was determined using the following formula:

$$s = \sqrt{\frac{1}{n-1} \sum_{i=1}^n (x_i - \bar{x})^2} \tag{2}$$

The FMJ bullets had a mean dispersion of 2.3 cm with a standard deviation of 5 mm, indicating high consistency and stability in flight. The HP bullets exhibited a mean dispersion of 31 mm with a standard deviation of 7 mm, suggesting slightly higher variability, likely due to their design, which can affect aerodynamic performance. The largest dispersion was observed with the SP bullets, with a mean value of 42 mm and a standard deviation of 10 mm, potentially caused by the deformation of the soft tip upon firing. Statistical analysis, including a t-test, showed that the differences between the mean dispersions of FMJ and HP bullets are statistically significant at the 5 % significance level (p-value 0.03), highlighting the importance of bullet shape for shooting accuracy.

A t-test was performed to compare the means of FMJ and HP bullets, resulting in a p-value of 0.03,

indicating a statistically significant difference at the 5 % significance level. A t-test was performed to compare the mean dispersions of FMJ and HP bullets, calculated as:

$$t = \frac{\bar{x}_1 - \bar{x}_2}{\sqrt{\frac{s_1^2}{n_1} + \frac{s_2^2}{n_2}}} \quad (3)$$

where x_1 and x_2 are the mean values, s_1 and s_2 are the standard deviations and n_1 and n_2 are the sample sizes for bullets respectively.

4 CONCLUSION

The results indicated significant differences in the dispersion patterns between the different bullet shapes. The FMJ bullets showed the tightest grouping, suggesting higher consistency and stability in flight. The HP bullets had a slightly larger dispersion, likely due to their design, which can cause variations in aerodynamic performance. The SP bullets exhibited the largest dispersion, which might be attributed to the softer tip deforming upon firing.

These findings align with previous studies that have highlighted the importance of bullet design in ammunition performance (Smith & Wesson, 2020; Brown, 2019). The higher dispersion of HP and SP bullets may also be linked to variations in manufacturing processes and material properties.

Furthermore, the analysis suggested that environmental factors, such as wind and temperature, had a minimal impact on the dispersion patterns observed. This reinforces the conclusion that bullet shape is a critical determinant of accuracy in .223 Remington ammunition.

References

- [1] CARLUCCI, E. and JACOBSON, S. *Ballistics: Theory and Design of Guns and Ammunition*. 2013. 612 pages. ISBN: 978-1-4557-3131-3. <https://doi.org/10.1201/b15495>
- [2] RINKER, A. *Understanding Firearm Ballistics*. 2018. 496 pages. ISBN: 978-1-61039-025-3.
- [3] SMITH, J. *Cartridge Reloading in the Twenty-First Century*. 2012. 320 pages. ISBN: 978-1-61608-832-2.
- [4] MCCOY, R. L. *Modern Exterior Ballistics*. U.S. Army Research Laboratory, 2005. Available at: <https://apps.dtic.mil/sti/pdfs/ADA441359.pdf>
- [5] DAKIN, J. and MURPHY, C. The Forensic Analysis of Ammunition and Ballistics. In *Journal of Forensic Sciences*, 2021, 66(5), 1234-1245. Available at: <https://onlinelibrary.wiley.com/doi/full/10.1111/1556-4029.15152>

Dipl. Eng. Tomáš **RÁZGA**
Armed Forces Academy of General M. R. Štefánik
Department of Mechanical Engineering
Demänová 393
031 01 Liptovský Mikuláš
Slovak Republic
E-mail: tomas.razga@aos.sk

Dipl. Eng. Peter **BALÁŽ**
Armed Forces Academy of General M. R. Štefánik
Department of Mechanical Engineering
Demänová 393
031 01 Liptovský Mikuláš
Slovak Republic
E-mail: peter.balaz@aos.sk

Dipl. Eng. Michal **MOZOĽA**
Armed Forces Academy of General M. R. Štefánik
Department of Mechanical Engineering
Demänová 393
031 01 Liptovský Mikuláš
Slovak Republic
E-mail: michal.mozola@aos.sk

Dipl. Eng. Vratislav **KREHEL**
Armed Forces Academy of General M. R. Štefánik
Department of Mechanical Engineering
Demänová 393
031 01 Liptovský Mikuláš
Slovak Republic
E-mail: vratislav.krehel@aos.sk

Tomáš RÁZGA was born in 1995 in Ružomberok. He is currently studying internal PhD. at Department of Mechanical Engineering in Armed Forces Academy of General M. R. Štefánik. His research area mainly includes small arms and ammunition.

Peter BALÁŽ was born in 1995 in Liptovský Mikuláš. He received his M.Sc (Eng.) at the Armed Forces Academy in Liptovský Mikuláš in 2020. He started his dissertation studies in 2023 at Department of Mechanical Engineering in Armed Forces Academy of General M. R. Štefánik. His research area mainly includes small arms and ammunition.

Michal MOZOĽA was born in Krupina, Slovakia in 1988. He received his M. Sc (Eng.) at the Armed Forces Academy in Liptovský Mikuláš in 2017. He started his dissertation studies in 2022. His research interests are focused on the optimisation of automatic weapon fire modes. He is currently working as an assistant professor at the Department of Mechanical Engineering in Armed Forces Academy of General M. R. Štefánik in Liptovský Mikuláš.

Vratislav KREHEL was born in Liptovský Mikuláš, Slovakia in 1972. He received his M.Sc (Eng.) at the Military Academy in Liptovský Mikuláš in 2003. He started his dissertation studies in 2021. His research interests are focused on optimization of sniper weapons fire mode. He is currently working as an assistant professor at the Department of Mechanical Engineering in Armed Forces Academy of General M. R. Štefánik in Liptovský Mikuláš.



ROCKET ENGINES' SOLID PROPELLANTS AND COMBUSTION PRODUCTS

Martin KŘEPSKÝ

Abstract: Rocket technology has shown considerable progress in recent decades. In addition to peaceful use, rockets are used in the military as a means of transporting destructive charges on a target. Any information obtained, even a partial one, could be used to prevent or mitigate a missile threat. Different types of rocket engines are sources of rocket propulsion. One of the factors by which individual types of rockets differ from each other is the type of fuel used. Combustion of rocket fuel creates a flame that is a source of radiation. The article analyzes the composition of different types of solid propellants and their combustion products. It is further considered if combustion products detected via emission spectra can indicate the rocket launch and if it is possible to identify the type of rocket by assignment of emission spectra to known propellant. The recherche of multiple sources is the method used for gathering information concerning rocket propellants. The results of the recherche are the most used propellants' compositions and their combustion products.

Keywords: Rocket engines; Solid propellants; Combustion products; Emission spectrum.

1 INTRODUCTION

In nowadays conflicts, rockets and missiles cause significant numbers of casualties. Timely warning and defensive measures could decrease the casualties when the rockets and missiles are detected. Thus knowing the details i.e. type of the rocket and the trajectory can increase level of protective measures. The rocket engine is one of the limiting factors of trajectory and maximum range.

Structurally, the rocket consists of various parts. One of the main parts that give the rocket propulsion is the rocket engine with different types of fuel. Combustion of the fuel results in the formation of fumes that flow out of the rocket engine nozzle and create the necessary thrust to drive the system. If "exotic" types of rocket fuel such as a nuclear source are omitted, the fuels can be divided into two main groups: liquid propellants and solid propellants. The existence of a hybrid propulsion method, i.e. a combination of liquid and solid rocket fuel components, is possible.

A flame emitting optical radiation is created during the chemical reactions taking place as part of the burning process. Combustion is a chemical reaction where fuel is oxidized with the help of an oxidizing agent. The spectral distribution of optical radiation intensities at different wavelengths depends on the chemical composition of substances and the burning conditions. The objective of the article is to find out whether rocket solid propellants of different chemical structure effect combustion products and what is the composition of the products. If composition of combustion products differs, the differences will be affecting emission spectra. The analysis of obtained emission spectra could provide supplementary information to air defence process.

Solid propellants can be divided according to different criteria. The basic division can be into homogeneous solid propellants and heterogeneous

solid propellants. Further breakdown by chemical composition is given below.

2 HOMOGENEOUS SOLID PROPELLANTS

In the case of homogeneous solid propellants, the propellant grains are usually of larger dimensions than the dimensions of the grains of ordinary gunpowder. In terms of chemical composition, it is nitrocellulose, which absorbs a certain amount of nitroglycerin and other additives. Sometimes these propellants are called double-base propellants. Because both components, nitrocellulose and nitroglycerin, are hydrocarbons containing a significant amount of oxygen, the mixture acts as both a fuel and an oxidizer. The next stage of improving the properties of these mixtures is the addition of explosive components such as nitramines, e.g. RDX or HMX. Furthermore, part of the nitrocellulose can be replaced by another binder, most often a polymer, which gives the mixture elastic properties that increase the resistance of the propellant grain [1, p. 493 – 494].

The composition of nitroglycerin gunpowder-based rocket fuels of different origins in World War II. is shown in Table 1 [2, pp. 405 – 407]. Other energy components than nitroglycerin are added into the mixture e.g. German Giessling Pulver or Nebelwerfer mixtures. The percentages in brackets given for nitrocellulose express the nitrogen content by weight.

3 HETEROGENEOUS SOLID PROPELLANTS

Heterogeneous solid propellants are formed by a mixture of powdered metal, most often aluminum, and inorganic oxygen-rich salts, such as ammonium perchlorate, joined together by a liquid polymer binder, which is then cured. Common heterogeneous mixtures contain 60-72 % ammonium

perchlorate and up to 22 % aluminum powder. Organic binder - polymer is represented in 8-16 %. Further modification of these mixtures can be achieved by adding the already mentioned nitramines (RDX, HMX) or nitroglycerin. The nitramines increase the performance parameters of the mixture. Part of the ammonium perchlorate and polymer can be replaced by other high-energy substances [1, p. 493 – 494]. For the sake of extensiveness and to maintain clarity, the compounds of the individual components of solid propellants are not listed in full. An illustrative list is given in Table 2 [1, p. 514 – 515]. The components that can affect the composition of combustion products are listed above all.

Probably the oldest heterogeneous mixture used as a fuel is a mixture of asphalt and potassium

perchlorate called galcit 53. Asphalt, as a mixture of hydrocarbons, performed the function of fuel in the mixture, and perchlorate supplied the oxygen needed for its combustion [2, pp. 405 – 407]. Asphalt was later replaced by polymer binders such as Thiokol or polymethyl methacrylate (PMMA). The conditions imposed on these binders are high mechanical resistance and elasticity. The most used oxidizing agents in heterogeneous mixtures are potassium nitrate, ammonium nitrate, potassium perchlorate and ammonium perchlorate. Some properties of heterogeneous solid propellant based on PMMA – potassium perchlorate are listed in Table 3 [2, p. 405 – 407].

Tab. 1 Composition of World War II. rocket fuels based on nitroglycerin gunpowder

Name of propellant	Composition of propellant	
	Name of item	[% wt.]
Soviet Union (I.P.)	Nitrocellulose (13,75 % N)	52,2
	Nitroglycerin	43,0
	Diethyl phthalate	3,0
	Diphenylamine	0,6
	Potassium nitrate	1,1
	Nigrosin	0,1
Soviet Union (I.P.N.)	Nitrocellulose (13,25 %)	51,5
	Nitroglycerin	43,0
	Diethyl phthalate	3,0
	Centralite	1,0
	Potassium sulfite	1,25
	Soot	0,20
	Candela wax	0,05
Soviet Union (Slow burning gunpowder)	Nitrocellulose (12,2 %)	56,5
	Nitroglycerin	28,0
	Dinitrotoluene	11,0
	Centralite	4,4
	Candela wax	0,1
Great Britain	Nitrocellulose	41,0
	Nitroglycerin	50,0
	Centralite	9,0
Germany (Giessling Pulver)	Nitrocellulose	28,0 – 30,0
	Trinitrotoluene	50,0 – 52,0
	Diethylene glycol dinitrate	17,0 – 18,0
	Centralite	0,5
	Diphenylamine	0,5
Germany (Nebelwerfer)	Nitrocellulose	63,0
	Diethylene glycol dinitrate	35,0
	Centralite	0,5
	Wax	0,2
	Graphite	1,2
Japan	Nitrocellulose	60,0
	Nitroglycerin	27,0
	Nitronaphthalene	7,0
	Centralite	3,0
	Potassium sulfite	3,0

Source: [2].

Tab. 2 Overview of typical components of heterogeneous solid propellants

Item	Content [%]	Abbreviation	Chemical substance
Oxidizers	0 - 70	AP AN KP KN ADN	Ammonium perchlorate Ammonium nitrate Potassium perchlorate Potassium nitrate Ammonium dinitramide
Metal fuels	0 - 30	Al Be Zr	Aluminum Beryllium (experimental only) Zirconium (also burn-rate modifier)
Fuels/binders polybutadiene type	5 - 18	HTPB etc.	Hydroxyl-terminated polybutadiene
Fuels/binders polyether or polyester type	0 - 15	PU etc.	Polyurethane polyether or polyester
Curing agents or crosslinkers	0,2 – 3,5		
Burn-rate modifiers	0,2 – 3,0	FeO	Ferric oxide Oxides of Cu, Pb, Zr, Fe Alkaline earth carbonates Alkaline earth sulphates Metallo-organic compounds
Explosive filler	0 - 40	HMX RDX NQ	Octogen Hexogen Nitroguanidine
Plasticizers	0 – 7		
Energetic plasticizer (liquid)	0 - 14	NG DEGDN TEGDN TMETN	Nitroglycerin Diethylene glycol dinitrate Triethylene glycol dinitrate Trimethylolethane trinitrate
Energetic fuel/binder	0 - 15		
Processing aid, stabilizers, etc.	< 0,5		Lecithin

Source: [1].

Tab. 3 Properties of heterogeneous solid propellants based on PMMA – potassium perchlorate

Composition of propellant [% wt.]		Density [g.cm ⁻³]	Heat of combustion [kJ.kg ⁻¹]	Temperature of flame [K]	Burn-rate under the pressure [cm.s ⁻¹]		
PMMA	KClO ₄				30 atm	50 atm	100 atm
20,0	80,0	1,88	3 349,44	3750	1,41	-	-
22,5	77,5	1,88	3 483,42	3770	1,43	2,34	5,48
25,0	75,0	1,86	3 596,46	3778	1,38	2,33	-
30,0	70,0	1,82	3 466,67	3518	1,17	2,12	-

Source: [2].

It can be seen from Table 3 that by reducing the oxidizing agent in favor of the fuel, there is first a slight increase in the burning rate and then, at a certain concentration, its decrease. As the pressure in the combustion reaction zone increases, the burning rate will increase. Compared to nitrocellulose and nitroglycerin-based propellants, the burning temperature of the PMMA – potassium perchlorate mixture is much higher. The temperature of combustion has significant effect on radiation characteristics. The comparison of radiation source's and known sample's temperature difference

is a possible way for rocket recognition. The difference of combustion temperatures for the mixtures of same amount of oxidizer (80 % AP) and different fuel is depicted in Tables 3 and 4.

Another advantage of heterogeneous mixtures is higher chemical stability, unlike propellants based on smokeless powders, which contain components subject to decomposition reactions, especially at elevated temperatures. Some other examples and compositions of solid propellants are given in Table 4 [3, p. 212].

Tab. 4 Comparison of some properties of solid propellants

Propellant	Components	Density [10 ⁻³ , kg.m ⁻³]	Heat of combustion [MJ.kg ⁻¹]	Temperature of combustion [K]
Diethylene glycol-based propellant (dg)	Diethylene glycol, nitrocellulose, additives	1,55 – 1,60	3,726	2390
Nitroglycerin based propellant (ng)	Nitroglycerin, nitrocellulose, centralite, additives	1,61	5,149	3160
Galcit propellant	Potassium chlorate, asphalt (75/25)	1,74	-	1970
---	Ammonium nitrate, rubber, catalysator (80/18/2)	1,55	-	1720
---	Ammonium perchlorate, fuel, additives (80/20)	1,72	-	2790
---	Ammonium perchlorate, polyurethan	-	-	3300

Source: [3].

Contrary to the previous information, potassium chlorate and not potassium perchlorate is used as an oxidizing agent in Galcit propellant.

4 PRODUCTS OF COMBUSTION

Rocket propellant composition determines combustion products. The following text describes the major changes of combustion products content based on reactants.

At concentrations of ammonium perchlorate above 70 % in the mixture, the combustion products contain significant amounts of H₂O and O₂. Hydrochloric acid is also present in gas products in the range of 10 – 20 % mol. (exceptionally it exceeds 14 % for common fuels). The other products, CO, CO₂ and H₂, tend to decrease. Change of ammonium perchlorate content in the examined range of 60 – 100 % mol. does not affect the amount of nitrogen (5 – 10 % mol.) in the flue gas. In the second case, when the mixture contains RDX instead of ammonium perchlorate, the waste products contain C, CO, CO₂, H₂, H₂O and N₂. Above 80 %

RDX content, there is a decrease in C, CO and H₂ and an increase in CO₂ and H₂O [1, pp. 503, 505].

Combustion products of solid propellants composed of ammonium perchlorate and polybutadiene-based fuel terminated with a hydroxyl group (Hydroxyl Terminated Polybutadiene - HTPB) at pressure lower than atmospheric form a mixture of 16 stable elements and compounds. Those products are HCl, H₂O, CO, NH₃, CO₂, HClO, NO, O₂, H₂, NO₂, N₂, C₄H₆, C₂H₂, ClO₂, Cl₂, and HCN [4, pp. 342 – 343].

In the case of RDX burning (at pressure lower than atmospheric), the products are HCN, NO, H₂O, HNCO, H₂, N₂, CO, CO₂, N₂O, NO₂, when the first-mentioned HCN and NO further react together and their concentrations reduces. Combustion of HMX at atmospheric pressure then provides similar products HCN, NO, H₂O, N₂, CO₂, NO₂ and CH₂O [4, pp. 343 – 344].

When burning, the substance ammonium dinitramide (ADN) produces the fumes listed in Table 5. The different composition of the fumes depends on the distance from the burning surface

and the ambient pressure. ADN mixed with HTPB then provides waste products with the composition shown in Table 6 [4, p. 345, 347, 349]. It is worth noting the differences in the composition of the combustion products of ADN at a pressure

of 6 atm (Tab. 5) and the final combustion products (Tab. 6). This difference can be attributed to other reactions taking place at a greater distance from the combustion zone.

Tab. 5 ADN combustion products

p = 6 atm, distance from the burning surface L = 4,4 mm							
Items	NH ₃	NO	N ₂ O	N ₂	HNO ₃	H ₂ O	ADN
Content [%]	0,07	0,23	0,28	0,10	0,02	0,30	0,00
p = 3 atm, distance from the burning surface L = 0,2 mm							
Items	NH ₃	NO	N ₂ O	N ₂	HNO ₃	H ₂ O	ADN
Content [%]	0,08	0,19	0,24	0,08	0,08	0,30	0,03

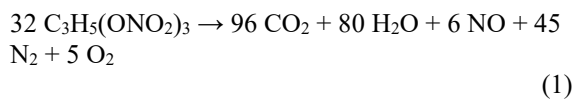
Source: [4].

Tab. 6 Combustion products of ADN and mixtures of ADN and HTPB

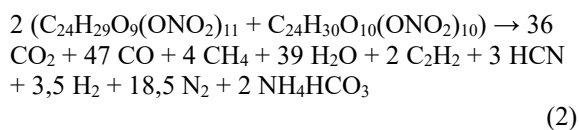
Composition	p [atm]	T [K]	NH ₃	H ₂ O	N ₂	NO	N ₂ O	CO ₂
ADN/HTPB (97/3)	1	2370	0,01	0,35	0,13	0,26	0,18	0,06
ADN	6	1420	0,00	0,45	0,11	0,25	0,20	---

Source: [4].

In the case of nitroglycerin alone, the explosive decomposition can be expressed as follows:



During the reaction, the explosion heat of 6,091.79 kJ.kg⁻¹ is released, the specific gas volume V₀ is 715 l.kg⁻¹ and the explosion temperature is 4250°C [5, p. 27]. Nitrocellulose with a nitrogen content of 13.1 % decomposes according to the equation below [5, p. 175].



Similar compositions of the combustion products of the compounds contained in rocket propellants are shown in Table 7. Only the main components of the combustion products are shown. In the case of nitrocellulose, the difference in the composition of the combustion products is largely influenced by the different amounts of nitrogen in the original composition. In the case of nitroglycerin, in contrast to Table 7, CO is not listed as a product of the reaction in the decomposition equation, and on the contrary, NO is listed as a product of nitrogen oxidation [6, p. 21]. In addition to nitrocellulose, nitroglycerin, ammonium perchlorate and ammonium nitrate, some other compounds are listed in Table 7.

Tab. 7 Combustion products NC, NG, AP, AN

	Composition [moles/mole]								
	O ₂	H ₂ O	CO	CO ₂	H ₂	N ₂	HCl	Cl ₂	OH
NC (12,6 % N)		0,225	0,147	0,128	0,116	0,111			
NG	0,069	0,280	0,107	0,275	0,014	0,181			0,041
TMETN		0,263	0,357	0,096	0,140	0,136			
TEGDN		0,110	0,397	0,063	0,335	0,079			
DEGDN		0,253	0,365	0,079	0,190	0,111			
AP	0,287	0,377				0,119	0,197	0,020	
AN	0,143	0,571				0,286			
NP	0,750					0,125		0,125	
RDX		0,226	0,246	0,082	0,089	0,326			
HMX		0,227	0,246	0,082	0,089	0,326			

Source: [6].

The values of the composition of the combustion products of various solid propellants of the ICT

Thermodynamic Code calculation model are shown in Table 8 [7, p. 154].

Tab. 8 Combustion products of various solid propellants according to the ICT Thermodynamic Code calculation model

Type of propellant	Environment Pressure [MPa] Temperature [K]	Composition [% wt.]							
		CO ₂	H ₂ O	N ₂	CO	H ₂	Cl	OH	HCl
Nitramine (85 % HMX, 15 % binder)	inert 10 MPa 2293 K	5,931	9,132	32,551	49,946	2,421			
	air 0,1 MPa 1227 K	27,700	10,111	62,168	0,001	0,000			
Double-based solid propellant (50 % NC (13.3 % N), 35 % NG, 11 % Triacetin, 2 % Centralite, 2 % CuO)	inert 10 MPa 2508 K	21,790	17,215	13,332	45,021	1,008			
	air 0,1 MPa 1317 K	37,832	10,746	50,743	0,013	0,000			
Heterogenous solid propellant (80 % AP, 10 % Al, 10 % binder)	inert 10 MPa 3470 K	8,362	20,720	9,509	14,724		2,332	1,487	22,166
	air 0,1 MPa 1909 K	19,647	18,089	34,100	0,228		0,261	0,034	15,492

Source: [7].

Modeling of chemical reactions was carried out for two different states of the surrounding environment. In the case of modeling reactions in air, subsequent reactions occur, which correspond to a change in the composition of the waste products, e.g. a decrease in CO and an increase in CO₂ by subsequent oxidation, the formation of N₂, in the case of heterogeneous solid propellants, a decrease in the content of Cl radicals. The resulting permeability of double-based solid propellant emissions is higher than that of heterogeneous solid propellant. The spectral dependence of the transmittance of double-based solid propellant emissions shows a decrease at wavelengths of 4.25 μm (CO₂ absorption), in the range of 4.70 – 4.90 μm (CO absorption) and below 3.00 μm (H₂O absorption). On the contrary, heterogeneous solid propellant shows permeability only in the range of 8.00 μm – 10.0 μm [7, p. 155].

The emission spectrum of the double-based solid propellant also differs from the heterogeneous one. The double-based solid propellant shows higher values of the spectral dependence of the intensity of the emission spectrum compared to the values of the heterogeneous solid propellant in the infrared region. This difference is caused by the different

number of particles produced in the combustion gases. In the case of the infrared part of the spectrum, these are CO₂ and H₂O particles [8, p. 188].

In the case of solid propellant with the highest useful values, it is a heterogeneous solid propellant based on a mixture of ammonium perchlorate and aluminum powder. Mixtures of ammonium perchlorate and aluminum have a significant disadvantage in the amount of waste products produced, where a significant part consists of Al₂O₃ as a product of oxidation [9, p. 84 – 85].

5 CONCLUSION

Comparison of information provided in multiple free-accessible sources was used to list the main combustion products of solid rocket fuels.

Based on the above-mentioned different types of solid propellants, it is possible to identify the typical components used in individual mixtures. In the case of double-based mixtures, it is nitrocellulose and nitroglycerin with the main combustion products H₂O, CO₂ and N₂. In the case of nitroglycerin, then O₂. In nitramines (RDX and HMX), in addition to the previous ones, CO is also represented. Heterogeneous perchlorate-based

solid propellant produces Cl radicals or an HCl compound. The waste products of mixtures containing powdered metal, e.g. Al, contain oxides of these metals. The combination of these products in exhaust depends on the original solid propellant composition (qualitative and quantitative). On the contrary, some emission spectrum implies the combustion products of propellants. The surrounding atmosphere must be considered for its effects on observation. If the emission spectrum is detected and the surrounding conditions are known, it would be possible to determine the original substances. If the original composition of rocket propellant is known the reverse approach can be utilized to identify the rocket by its combustion products.

References

- [1] SUTTON, George P. and BIBLARZ, O. *Rocket Propulsion Elements*. 8th Edition. Hoboken: John Wiley, ©2010. ISBN 978-0-470-08024-5.
- [2] URBAŃSKI, T. *Chemie a technologie výbušin III*. díl. Praha: SNTL, 1959. ISBN L 16-B3-4-II/6270.
- [3] KROULÍK, J. a RŮŽIČKA, B. *Vojenské rakety*. Praha: Naše vojsko, 1985. ISBN 28-067-85.
- [4] KOROBENICHEV, Oleg P. Flame Structure of Solid Propellants. In: BRILL, Thomas B., Wu-Zhen REN a Vigor YANG. *Solid Propellant Chemistry, Combustion, and Motor Interior Ballistics*. Reston: American Institute of Aeronautics and Astronautics, © 2000, s. 335-354. Progress in Astronautics and Aeronautics, Volume 185. ISBN 978-1-56347-442-2.
- [5] URBAŃSKI, T. *Chemie a technologie výbušin II*. díl. Praha: SNTL, 1958. ISBN L 16-B3-4-II/6245.
- [6] KUBOTA, N. Survey of Rocket Propellants and Their Combustion Characteristics. In: KUO, Kenneth K. and SUMMERFIELD, M. *Fundamentals of Solid-propellant Combustion*. New York: American Institute of Aeronautics and Astronautics, © 1984, s. 1-52. ISBN 0-915928-84-1. Available at: <https://doi.org/10.2514/5.9781600865671.0001.0052>
- [7] DEIMLING, L., LIEHMANN, W., EISENREICH, N., WEINDEL, M. and ECKL, W. *Radiation Emitted from Rocket Plumes*. Propellants, Explosives, Pyrotechnics. © 1997, 22(3), 152-155. ISSN 0721-3115. Available at: <https://doi.org/10.1002/prep.19970220310>
- [8] BLANC, A., DEIMLING, L. and EISENREICH, N. *UV - and IR-Signatures of Rocket Plumes*. Propellants, Explosives,

Pyrotechnics. © 2002, 27(3), 185-189. ISSN 0721-3115. Available at: [https://doi.org/10.1002/1521-4087\(200206\)27:3<185::AID-PREP185>3.0.CO;2-H](https://doi.org/10.1002/1521-4087(200206)27:3<185::AID-PREP185>3.0.CO;2-H)

- [9] FLEEMAN, Eugene L. *Tactical Missile Design*. Reston: American Institute of Aeronautics and Astronautics, ©2001. ISBN 1-56347-494-8.

Dipl. Eng. Martin **KŘEPSKÝ**
JCBRN Defence COE
Víta Nejedlého
682 01 Vyškov
Czech Republic
E-mail: martin.krepsky@unob.cz

Martin KŘEPSKÝ, born in 1980, is absolvent of Military Academy in Brno (2003) and University of Pardubice (2021). After the graduation from Military Academy he has been assigned to different command and training posts of the Armed Forces of the Czech Republic. His interest is in optoelectronic means of detection and identification of chemical agents.

SCIENCE & MILITARY - WRITER'S GUIDELINES

1. Scientific articles submitted for publishing have to be original, topical and never been published before.
2. Articles have to be written in English language and in accordance with ethical standards. For more details, please visit the website of the Science & Military Journal (<http://sm.aos.sk/index.php/en/ethical-standards>).
3. Length of the article should not exceed 6 pages in defined format. Microsoft Word text editor must be used for writing. Articles must be written using Times New Roman, single line spacing and follow the following form: Title - 12 point bold capital letters aligned to the center. Full author's (co-author's) name – 10 point normal letters aligned to the center. Abstract – 9 point normal letters, extent 3-5 lines. Keywords – 9 point normal letters. The article text – 10 point normal letters. Contact - full author's (co-author's) name, affiliation, e-mail – 9 point normal letters at the end of the article. The article text will be written in 2 columns format with a 75 mm column width and 10 mm empty space separating the columns. The first line of each paragraph must be shifted 5 mm to the right.
4. Upper and lower margins must be set to 25 mm, left and right margins to 20 mm. Select mirror margins and set binding margins to 10 mm. The distance between the header/footer and the page margin must be 12,5 mm, while different odd and even pages must be selected.
5. Photographs for publication must be in black-white (not in color) of excellent quality with good contrast.
6. Equations in the text are also to be written using the equation editor. (Equation must be typed in Microsoft Equation, which is an integral part of Microsoft text editor.) They must be numbered. Numbers are to be enclosed in parentheses and aligned to the right margin of a column.
7. Figures, graphs and tables must be included in the text and numbered and must contain description. Figures must be identified as Fig. 1 followed gradually by the figure description. Graphs must be identified as Graph 1 followed by the graph description. Tables must be identified as Tab. 1, followed by the table description.
8. References must be fully and accurately documented (according to ISO 690). References should be quoted in the text in square brackets and listed in the order they have appear in the text.
9. The specimen article that can be found on the web-site: <http://sm.aos.sk/index.php/en/for-authors-en> can be used as an example of the correct format.
10. The editorial board will consider submitted articles in the next scheduled meeting. If it decides to include the article in the next issue it submits the manuscript to the editors for the peer review. The final version (before printing) will be sent to the author for the final revision. The authors are fully responsible for the level of language.
11. Contributions in A4 format edited according to the specimen article should be submitted in one hard copy and also in electronic form to the Editorial board.
12. The deadlines for the delivery of the articles in calendar year are: March 1 and September 1.

Content

Editorial 3

Chi Toan DANG, Van Bac DOAN
**A DESIGN OF 4-LENS THERMAL IMAGING OBJECTIVE WORKING
IN THE LWIR SPECTRAL REGION** 5

Bence HAJÓS
**SOME ADDITIONAL ASPECTS FOR THE REGULATION OF THE MILITARY LOAD CLASSIFICATION
OF EXISTING ROAD BRIDGES (STANAG 2021)** 14

Vratislav KREHEL', Michal MOZOĽA, Martin KŘEPSKÝ
MATERIALS AND TECHNOLOGIES IN THE DESIGN OF MILITARY OPTICAL DEVICES 20

Tomáš RÁZGA, Peter BALÁŽ, Michal MOZOĽA, Vratislav KREHEL'
INFLUENCE OF BULLET SHAPE ON .223 REMINGTON AMMUNITION ACCURACY ANALYSIS 29

Martin KŘEPSKÝ
ROCKET ENGINES' SOLID PROPELLANTS AND COMBUSTION PRODUCTS 36